Thermodynamic Interactions toward Nanocellulose Colloidal Properties

Aban Mandal

A thesis

submitted in partial fulfillment of the

requirements for the degree of

Master of Science

University of Washington

2023

Committee:

Eleftheria Roumeli

Navid Zobeiry

Program Authorized to Offer Degree:

Materials Science and Engineering

University of Washington

Abstract

Thermodynamic Interactions toward Nanocellulose Colloidal Properties

Aban Mandal

Chair of Supervisory Committee:

Eleftheria Roumeli

Department of Material Science and Engineering

In recent years, nanocellulose has emerged as a sustainable and environmentally friendly alternative to traditional petroleum-derived structural polymers. However, the widespread implementation of nanocellulose is hindered by the need for energy-intensive extraction and processing methods, limited quality reliability, and cost-effectiveness. In addition, the required fundamental understanding of process parameters that govern the morphology and structure-property relationships of nanocellulose systems, from colloidal suspensions to bulk materials, has not been developed and generalized for all forms of cellulose. This further hinders the more widespread adoption of this biopolymer in applications.

This thesis aims to investigate how cellulose nanofibers (CNFs) disperse in solvents with different thermodynamic parameters. The objective is to highlight how thermodynamic interactions can be changed to tune the colloidal behavior of CNF dispersions. By adjusting the Hansen solubility parameters, the thermodynamic interaction between CNFs and solvents has been controlled. Here, we obtained CNFs from bacterial cultures to examine the hydrodynamic, electrokinetic, and thermodynamic effects that control the colloidal behavior of CNFs in different solvents. We varied the concentration of CNFs to explore dilute to semi-dilute regimes for each solvent.

Specific viscosity was used to identify concentration-based transitions and compare the dispersions

with different interaction parameters. This provided insights into how CNFs respond to different solvents. The excluded volume and viscosity were found to increase when there was a higher interaction between CNFs and solvents in dilute concentrations. This showcases the impact of the balance between CNF-CNF and CNF-solvent interactions on the colloidal properties.

Deviations were noted in semi-dilute regimes due to weaker electrostatic stabilization and van der Waals attractions. These facilitate hydrocluster formation, which was confirmed via zeta potential measurements. Rheological characterization showed shear rate-based transitions, concentration effects on zero shear viscosity, stress overshoots, and viscoelasticity. This provides a foundation for phase behavior analysis and future implementation in structure-property relationships.

Our findings provide a thermodynamic understanding of CNF colloidal properties with minimal surface charge density, that enable aggregation due to insufficient electrostatic repulsion, This work elucidates the intricate interplay of thermodynamic and electrokinetic interactions toward understanding and controlling the colloidal behavior of nanocellulose.

Graphical Abstract:

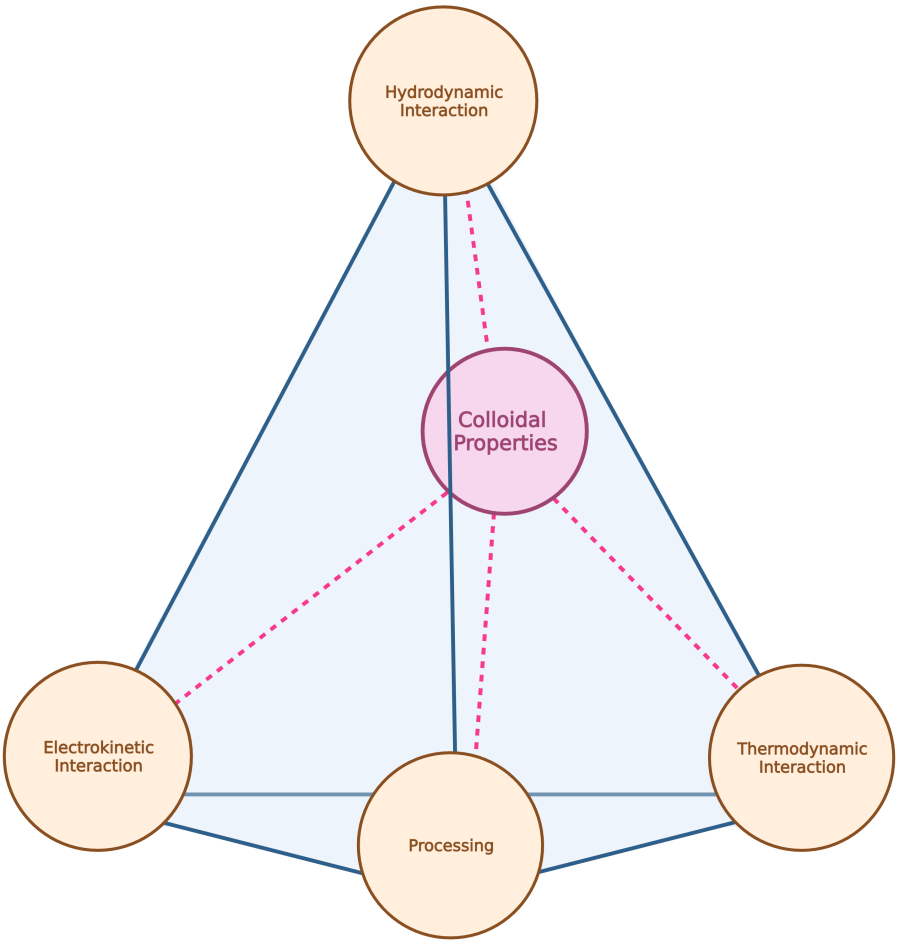

University of Washington
Graduate School

This is to certify that I have examined this copy of a master's thesis by:

Aban Mandal

And have found it complete and satisfactory in all respects,

and that any and all revisions required by the

final examining committee have been made.

Committee Members:

Prof. Eleftheria Roumeli

Prof. Navid Zobeiry

Date:

by any means shall not be allowed without my written permission.

Signature:

Date:

Contents

Page

Abstract

Contents **i**

List of Tables **iii**

List of Figures **iv**

1 Introduction **1**

1.1 Theoretical Background 1

1.1.1 Bonding and Structure 1

1.1.2 Thermodynamic forces 2

1.1.3 Electrokinetic forces 5

1.1.4 Hydrodynamic forces 6

1.1.5 Ordering in Colloidal Dispersions and their Hydrodynamic Response . . . 7

1.2 Phase behavior and transformation in nanocellulose dispersion 9

1.2.1 Thermodynamic Stabilization: Hansen Parameters Based dispersibility of CNFs 9

1.2.2 Electrostatic stabilization 10

1.2.3 Phase Behaviour of Nanocellulose Colloidal Dispersion 12

1.3 Objectives and Thesis Overview 17

2 Materials and Methods **20**

2.1 Materials 20

2.2 Experimental Methods 20

2.2.1 Growth of Bacterial Cellulose 20

2.2.2 Preparation of Bacterial Cellulose Colloidal Dispersion 20

2.2.3 Preparation of Bacterial Cellulose Films 20

2.3 Characterization Methods 21

2.3.1 Scanning Electron microscopy 21

2.3.2 Optical microscopy 21

2.3.3 Surface Charge Density Measurements 21

2.3.4 Zeta Potential 21

2.3.5 Rheological Methods 22

3 Characterization of Cellulose Nanofibers **23**
3.1 Results and Discussion 23
3.1.1 Zeta Potential and Surface Charge Measurements 23
3.1.2 Rheology 25
3.2 Conclusion 29

4 Cellulose Nanofiber Colloidal Properties **31**
4.1 Results and Discussion 31
4.2 Conclusion 35

5 Thesis conclusions **37**

6 Future Outlook **38**

References **39**

List of Tables

1 Carreau Fitting Parameters 26
2 Table summarising the Zeta Potential for CNF dispersions in different solvents . . 35

List of Figures

1 Bonding and Hierarchical Structure of cellulose,CNF and CNC, adapted from Fiorati et.al[1] 2

2 Concentration based transitions in nanocellulose colloidal dispersions , adapted from Benselfelt et.al [2] 14

3 Schematic representation summarizing the key methodologies involved 21

4 SEM Image of CNF dispersion (left), Optical Microscopic Image of CNF Dispersion (right) 23

5 Conductometric Titration for the Surface charge Density Determination (a,b),Zeta Potential Variation with pH (c) 24

6 Viscous Response of CNF Dispersions, Viscosity vs Shear Rate Full Range (top left), Viscosity vs Shear Rate in Low Shear Regime(bottom left), Viscosity vs Shear Rate in High Shear Regime(bottom right), Optical Images of CNF agglomerates/hydroclustes after application of High Shear (top right) 25

7 Carreau Model fitting (left), Zero Shear Viscosity Scaling with Volume Fraction (right) 27

8 Time-dependent Viscosity response under Constant Shear(a -e), Power law fitting of Viscosity response against Concentration and Time (f) 28

9 Loss and Storage Moduli over Strain Amplitude (a), Damping Factor(Tan δ) variation across Strain(b), Concentration Dependence of Loss and Storage Modulus at 1 % Amplitude and 1 rad/s Frequency(c), Frequency Sweep of Storage and Loss Modulus(d), Complex Viscosity against Frequency(e), Stress vs Strain(f) 29

10 Specific Viscosity of CNF Dispersion showing Concentration based regimes at $316s^{-1}$ in 100% Water(a),50% Water in DI (b) and 7.5% Water in IPA(c), Viscosity in mPa.s against Concentration in the 3 solvents(d), Specific Viscosity against Concentration in the 3 solvents(e), Zeta Potential and pH of CNF dispersion in 3 solvents without addition of any acid/base(f) 31

11 Relative of the different solvents across CNF volume fraction(left), highlight region of the graph on the right showing low volume fractions (left) 34

12 Solvent subtracted X-ray scattering profiles for 0.1 wt% CNF in the 3 different solvents. (right), Dimensionless(V_c) Kratky Plot (left) 34

1 Introduction

Cellulose nanofibers (CNFs) have recently emerged as a promising sustainable nanomaterial for advanced applications across diverse industries due to their remarkable mechanical properties, surface chemistry, abundance and environmental credentials[3, 4]. Derived from cellulosic biomass sources like plants and certain bacteria, CNFs bridge the worlds of green chemistry and sophisticated multifunctionality. However, effectively unlocking their nanoscale advantages requires a profound comprehension of their intricate colloidal dispersion behavior and resulting material performance.

1.1 Theoretical Background

1.1.1 Bonding and Structure

Cellulose forms high molecular weight chains of repeating β-D-glucopyranose monomers linked together by β-1,4 glycosidic bonds, these chains are bonded together through intra-chain and inter-chain hydrogen bonding forming cellulose fibrils, depending on the orientation of these chains, different type of crystalline or amorphous structures arise in cellulose. CNFs and CNCs are produced through cleaving this hierarchical structure through chemical, mechanical and/or enzymatic actions.

For the stability of colloidal dispersions, it is important to consider the secondary bonding present between the cellulose fibrils also known as the Van der Waals bonding. These bonds arise due to the London dispersive interaction between molecules and since we are considering CNFs and CNCs, these interaction potentials can be assumed to be like that of cylinders for simplicity, the limiting case for which is aligned and crossed and are given by the following equations [5, 6, 7].

$$V(D) = \frac{-AL\sqrt{R}}{24D^{3/2}} Aligned \tag{1a}$$

$$V(D) = \frac{-AR}{6D} Crossed \tag{1b}$$

Where A is the Hamaker's Constant, L is the length and R is the radius of the CNCs and CNFs, with a separation of D. In presence of a solvent, McLachlan showed that the Hamaker's constant is greatly modified and is related to the relative dielectric properties of the nanocellulose and the liquid. In a solvent medium Hamaker's Constant,A becomes [5, 8],

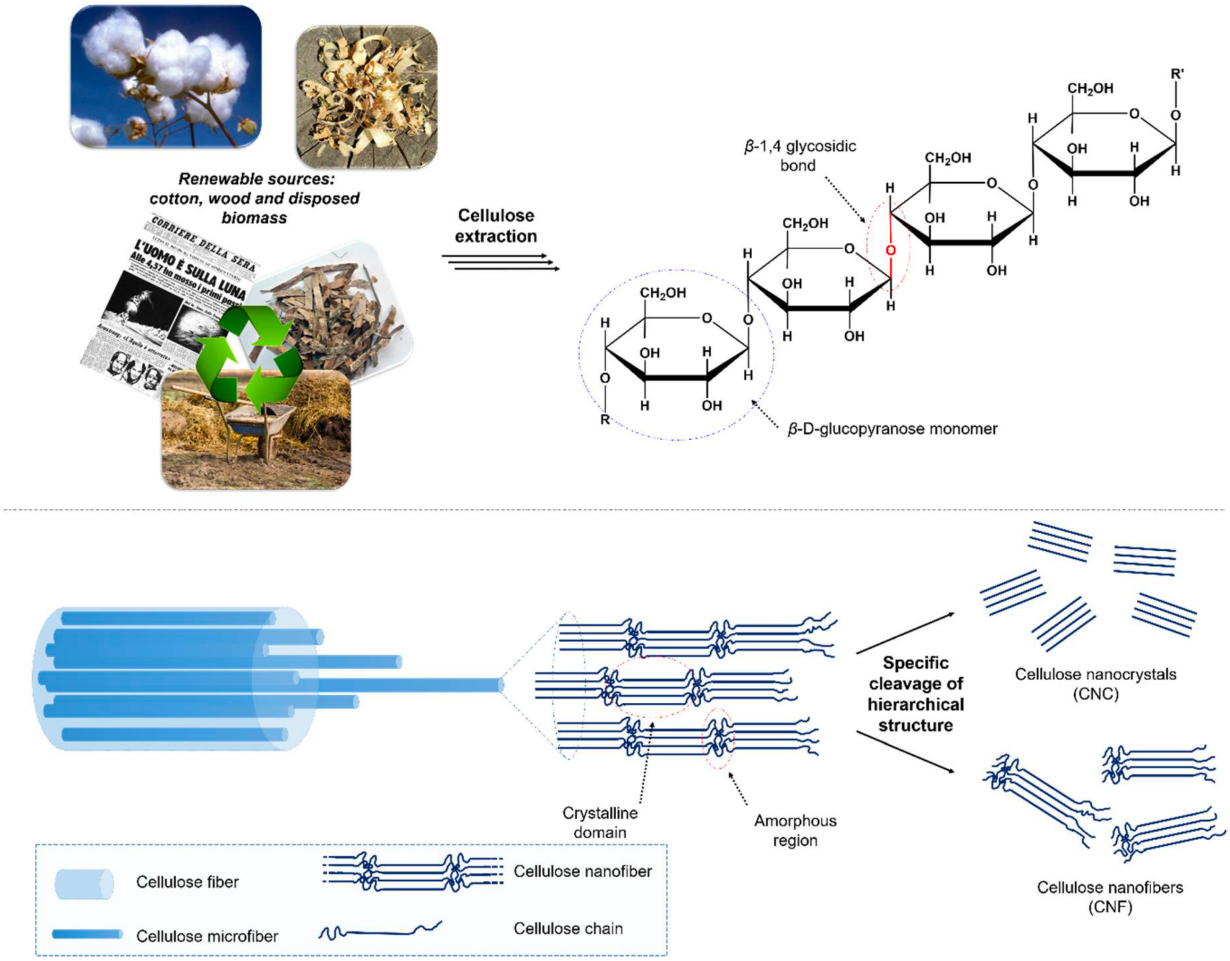

Figure 1: Bonding and Hierarchical Structure of cellulose,CNF and CNC, adapted from Fiorati et.al[1]

$$A = \frac{3I}{16\sqrt{2}} \frac{\left({n_A}^2 - {n_B}^2\right)^2}{\left({n_A}^2 + {n_B}^2\right)^{3/2}} \tag{2}$$

where n_A and n_B are the refractive index of the solvent and solute. In a liquid dispersion media, the attraction potential between the CNCs and CNFs is greatly modified, and aggregation in the nearby nanocellulose structures can be reduced by controlling the nanocellulose/liquid system such that the effective Van der Waals potential is lowered.

1.1.2 Thermodynamic forces

From the modified Hamaker's Constant in a liquid media, it can be observed that as n_A approaches n_B, the attractive potential and Hamaker's Constant approaches towards zero. This would mean that liquids with similar dielectric/optical properties to nanocellulose will result in no attractive potential, thus preventing nanocellulose aggregation and a stable colloidal dispersion. From the

above understanding, it can be concluded that Solute-Solvent interactions (relative to solute-solute and solvent-solvent interactions) is a key factor determining the stability of the dispersion. A strong solute-solvent interaction increases the energy cost of nanocellulose aggregation in the solvent as this would require displacing the solvent molecules at the solvent-nanocellulose interface, creating new surfaces. Thus, the aggregation of the nanocellulose will result in the increase of surface energy at the nanocellulose-solvent interface and this leads to a short-range repulsion around every nanocellulose bundle. The balance of these interaction energies is given by the Flory Huggins parameter, χ [5, 9].

$$\chi = -\frac{z}{2}\frac{\in_{AB} - \in_{AA} - \in_{BB}}{kT} \tag{3}$$

where,$\in_{AB}$,$\in_{AA}$,$\in_{BB}$ as the solute-solute, solute-solvent and solvent-solvent interaction energies.

Considering the Thermodynamics of binary mixing in the framework of a lattice model, the minimization of the free energy of mixing facilitates a stable dispersion of nanocellulose in a solvent, which is a function of the energetic and the entropic contribution to mixing. Using the lattice model, the energy of mixing is calculated by taking into consideration the pairwise interactions between the nanocellulose and the solvent as given by the Flory Huggins parameter, thus the enthalpy of mixing is given by[10]

$$\Delta H_{mix} = \chi\phi(1-\phi)kT \tag{4}$$

where ϕ is the polymer volume fraction, k is the Boltzmann constant, T is the temperature in Kelvin scale.The total entropy of mixing is calculated by considering the entropic contribution from each molecule in the system and is given by[9],

$$\Delta S_{mix} = -k[\frac{\phi_A}{N_A}\ln\phi_A + \frac{\phi_B}{N_B}\ln\phi_B] \tag{5}$$

where ϕ_A, ϕ_B is the polymer and solvent volume fractions and N_A,N_B is the molecular weight of the components A and B.

One of the fundamental considerations is that polymers are macromolecules with low molar mass solvent which defines the lattice, thus for polymer solutions N_A=N and N_B=1 and the ΔS_{mix} therefore becomes [9],

$$\Delta S_{mix} = -k[\frac{\phi_A}{N}\ln\phi_A + \phi_B\ln\phi_B] \tag{6}$$

It can be therefore understood from the deviations of equations 5 and 6 that for polymers the

entropic contributions to mixing are very small and diminish with increasing chain length of nanocellulose, despite that the entropy of mixing is always positive and promotes mixing. Another important consideration is that configurational entropy is identical in the dispersed and pure states(unmixed state, ie $\phi_{polymer} = 1$). Therefore, the Gibbs free energy of mixing is given by the Flory-Huggins equation for polymer solutions [9].

$$\Delta G_{mix} = kT[\frac{\phi}{N} ln\phi + (1-\phi)\ln(1-\phi) + \chi\phi(1-\phi)] \tag{7}$$

As described earlier the first two terms in equation 7 correspond to the entropic contributions and are very small to minimize ΔG_{mix}, however, they act to promote mixing, the third term is based on the energetic contributions and can be positive (opposes mixing), negative (promotes mixing) or zero depending on the Flory-Huggins Parameter χ. If the solute-solvent interaction is greater than the solute-solute and solvent-solvent interaction, $\chi < 0$, for all compositions a single-phase mixture is favorable, and if the solute-solute and solvent-solvent interaction is greater than the solute-solvent interaction, $\chi > 0$, mixing would not be favored. It needs to be noted that the equilibrium state of a dispersion at a particular composition depends on the functional dependence of the free energy on the composition which is guided by the Flory-Huggins Parameter and the degree of polymerization of nanocellulose.

Taking just the dispersion interactions into account (for non-polar dispersions), the interaction parameter χ, is related to the Hildebrand solubility parameter δ, which is the square root of the total cohesive energy density, such that[11, 9, 5]:

$$\chi = \frac{v}{kT}(\delta_A - \delta_B)^2 \tag{8}$$

where v is the lattice site volume.

Most systems have polar and specific hydrogen bonding interactions along with dispersive ones, thus taking the contributions from polar and hydrogen bonding interactions into consideration along with the Van der Waals forces, the Flory Huggins interaction parameter is modified using the Hansen Solubility Parameters for dispersive (δ_D), polar (δ_P) and hydrogen bonding (δ_H) [10]

$$\chi = \frac{v}{kT}[(\delta_{D,A} - \delta_{D,B})^2 + (\delta_{P,A} - \delta_{P,B})^2 + (\delta_{H,A} - \delta_{H,B})^2] \tag{9}$$

To compare the compatibility of a solvent and a material Skaarup and Hansen further developed an equation to calculate the solubility parameter distance, R, between two materials [12] given by

$$R = [4(\delta_{D,A} - \delta_{D,B})^2 + (\delta_{P,A} - \delta_{P,B})^2 + (\delta_{H,A} - \delta_{H,B})^2]^{1/2} \tag{10}$$

1.1.3 Electrokinetic forces

Colloid stabilization is frequently accomplished by development of surface charge on the colloidal particles. Deprotonating surface groups or adsorbing ions from the solvent can accomplish this. A diffuse layer of counter-ions from the liquid are then drawn to the surface charge. The concentration of counter-ions is highest near the solid surface and decreases with distance from the surface, while the concentration of charge-determining ions changes oppositely. This inhomogeneous distribution of ions near the solid surface leads to the formation of a double-layer structure. Since the counter-ions are diffuse, they provide an effective surface charge that repels other surrounding charged colloids by Coulomb repulsion and this potential is given by the zeta potential ζ. By providing a transient and reversible surface charge by the adsorption of charged molecules onto the nanocellulose.

Due to the double layer's existence, the nanocellulose attractive van der Waals potential is counterbalanced by the double layer's repellent potential. The DLVO theory, which describes the physics of the double layer, was initially developed independently by Verwey and Overbeek and Derjaguin. Although the repulsive potential is dependent on the charged surface's geometric characteristics, it typically has the shape $V_D = Be^{-\kappa D}$. The thickness of the double layer is indicated by the term κ^{-1} which is also known as the Debye screening length and is given by

$$\kappa^{-1} = \sqrt{\frac{(\varepsilon\varepsilon_{\circ} k_b T)}{2e^2 I}} \tag{11}$$

Where, $\varepsilon_{\circ}$ is the dielectric constant of the medium, ε is permittivity of free space, k_b is Boltzman Constant, T is the temperature in Kelvin scale and e is the elementary charge and I is the Ionic Strength. B typically relies on κ and ζ , and the surface's geometric characteristics and, in the case of cylinders, takes on a quite complicated form.

Both attractive and repulsive terms exist in the interaction potential between neighboring nanocellulose, the potential is given by [9, 13, 14, 15],

$$V_T(D) = -V_{VDR}(D) + Be^{-\kappa D}. \tag{12}$$

The attractive component is predominant at low separation distances creating a deep potential well, as the separation increases the potential well rises, forming a potential barrier, and then falls again as the separation widens. This potential barrier prevents agglomeration or aggregation in colloidal dispersions and is key for the stability of colloidal dispersions. The repulsive component in the equation is dependent upon the chemical environment, concentration of co-ion/ counter ions and other factors such as the presence of surfactants. It needs to be noted that these aforementioned factors affect the values of κ and ζ and thus when dispersion Nanocellulose in any solvent it is imperative to control the chemical environment and concentrations of species present in the disper-

sions such that κ and ζ are optimized to maximize the potential barrier to ensure the stability of the colloidal dispersion.

Another phenomenon of interest in the electrostatic interactions of colloidal dispersions is the counter ion condensation described through Manning's Theory which is also known as Mannings's Condensation. The dissociation of surface charge groups and their counter ions is dependent upon the compensation of the enthalpy loss due to favor entropy and the polarity of the solvent. In case such compensation is not enough the counterions condense on the charged group, such condensation has been also observed for water depending upon the ionic strength for nanocellulose dispersions.[16] The onset of counter condensation is related to the Bjerrum Length, λ_B, which is the separation at which for two elementary charges the electrostatic interaction is equal to thermal energy(k_bT), alternatively can be understood as minimum possible distance that two charges should be separated by before condensation occurs and is given by,

$$\lambda_B = \frac{e^2}{4\pi\varepsilon\varepsilon_\circ k_b T} \tag{13}$$

Where $\varepsilon_\circ$ is the dielectric constant of the medium, ε is permittivity of free space, k_b is Boltzman Constant, T is the temperature in Kelvin scale and e is the elementary charge. As the ionic concentrations of a colloidal dispersion increase, as we can see in Equation 11, the Debye length decreases, this results in a more localized electrostatic interactions with a decrease in the screening by the other ions present in the solution.[17] This causes the counter ion to approach the polyion and as the distance between the counterion and the polyion is less than the Bjerrum Length condensation of the counterion on the polyion [18] takes place to reduce free energy as having two charged groups close to each other is not energetically favorable. Such condensation leads to reduced double layer repulsion and this leads to agglomeration or network formation due to the prevalent Van der Waal's attraction.

1.1.4 Hydrodynamic forces

In a flow field due to the anisotropy of the particle the drag force exerted on the particles are anisotropic. The force exerted by the fluid on the particles depend on the orientation of the particles with respect to the flow field. Under shear flow rotation of the anisotropic particles takes place such that the particles align itself in the shear direction. The rotation slows down when the major symmetry axis is parallel to the shear direction as the torque experienced by the particle is minimized. The viscous response thus depends on the distribution of particle orientation as the stresses developed depends on how the particles are oriented. The Brownian motion tends to randomize the system and gives rise to a characteristic diffusion time such that the entropy of the system is increased, and the free energy is minimized. For rod-like structures both translational and rotational

motion contributes to the viscoelastic behavior of the dispersion. The particle anisotropy affects the equilibrium microstructure and phase behavior shifting the glass and gel transitions. Under shear flow, such alignments improve the packing fraction, reducing the viscosity. Thermal energy is the fundamental driving force of the colloidal dispersions creates a Hydrodynamic force on the particles, Stokes drag given by,

$$F^N = 6\pi\eta aV \tag{14}$$

where, η is the viscosity of the suspending medium, a is the the radius of gyration and V is the velocity of the particle, these interactions arise from the induced disturbances in the fluid flow due to the presence of the moving particle due to thermal motion and in turn affect other particles present in the flow field. For anisotropic particles, such as thermal and hydrodynamic interactions are guided by are aspect ratio since the motion of the particles due to these interactions would depend on the major symmetry axis.

1.1.5 Ordering in Colloidal Dispersions and their Hydrodynamic Response

The hydrodynamic response studied through the rheological behavior of colloidal dispersion is primarily dependent upon two factors: a) Aspect ratio and volume fraction of the particles,b) Surface potential and double layer thickness. The physical state of colloidal dispersions with rod-like particles is theoretically described by Onsager's Theory [19]. The free energy of rigid rod-like structures in the second virial coefficient limit is calculated from the Excluded volume average in the orientation distribution function denoted by ψ. If we consider two rods x and y with an angle of θ between them, the Helmholtz free energy per particle (energy normalized by kT) is given by,

$$f(\psi) = \int \psi(x)\left(ln(n.b.\psi(x) - 1)\right)dx + \frac{n}{2}\int E(x,y)\psi(x)\psi(y)dy \tag{15}$$

n is the number density; b is a constant and E refers to the Excluded Volume between the rods. The first part in the Equation 15 is the entropic component and the later refers to the second virial term. For large aspect ratio rods, the Excluded volume is expressed as,

$$E(x,y) = 2L^2 Dsin(\phi) \tag{16}$$

The Isotropic-Nematic transition is driven by entropy such that the Nematic Phase separates above a critical concentration, where both isotropic and nematic phases co-exist.
The presence of Double-layer repulsion affects the rod dimensions such that the length and diameter effectively become,

$$D_{eff} = D + \alpha\kappa^{-1} \tag{17a}$$

$$L_{eff} = L + \alpha\kappa^{-1} \tag{17b}$$

Under shear, rod-like structures along with translating in the flow direction, rotate and align relative to the direction of the flow. The zero shear and high shear Relative Viscosities can be quantitatively approached by Onsager's Method as described by Dhont and Briels[20]

$$\eta_{Relative,Pe\to 0} = 1 + \frac{8r^2}{45ln(r)}\phi \tag{18a}$$

$$\eta_{Relative,Pe\to \infty} = 1 + \frac{8r^2}{45ln(r)}\phi \tag{18b}$$

r is the aspect ratio.

For dispersions in the Semi dilute Regime, below the critical entanglement concentration i.e., prior to the entangled Semi Dilute Regime, the tube model proposed by Doi and Edwards can be appropriately applied where relative viscosity is given by,

$$\eta_{Relative} = 1 + \phi\frac{nL^3}{90}\ln r + \frac{\pi(nl^3)^3}{30\beta\ln r}$$

β is a constant that represents the constraints of the tube. Further works by Cassagnou et al[21] derived the ϕ^3 scaling of low shear viscosity when transitioning from dilute to the semi-dilute regime. Sato and Teramoto[22] taking into account entanglement extended tube model has been to concentrated regime for low shear relative viscosity, expressed through equation e,

$$\eta_{Relative} = 1 + \frac{\pi nL^3\ln r}{90} + \frac{\pi}{30\ln r}\left[1 + \frac{nL^3}{\sqrt{\beta}(\varepsilon ndL^2)}\right]^2 nL^3 \tag{19}$$

ε is the measure of entanglement. This correlation however is only limited to the liquid state, as the shear rate tends to 0 the viscosity of the volume arrested glassy state approach ∞.

1.2 Phase behavior and transformation in nanocellulose dispersion

1.2.1 Thermodynamic Stabilization: Hansen Parameters Based dispersibility of CNFs

The Hansen Parameters are the polar, dispersive, and hydrogen bonding components of cohesive energy density, it is key to highlight that aspect ratio, volume-to-surface area ratio, particle size morphology, crystalline structure of nanocellulose, the crystallinity index, and the surface modifications would greatly affect the Hansen Parameters. CNCs and CNFs have different crystalline polymorphs, Cellulose I-β polymorph, abundantly found in plant sources, has been the most studied polymorph thus far. The application of Hansen Parameters for the dispersibility of Nanocellulose can be understood through the understanding of the Hansen Parameters of the different crystal planes of the Cellulose I-β and other polymorphs. The polarity of the crystal planes depends on the polymorph considered[23, 24], hydrophilic (110) and $(1\bar{1}0)$ planes for Cellulose I-β,(100) for Cellulose I-α and (110) for Cellulose-II whereas the (200) planes for Cellulose I-β and (220) planes for Cellulose I-α and Cellulose II are hydrophobic. The relation between the Hansen parameters and crystalline planes has been studied for the Cellulose I-β by Bruel. et.al [25] as shown in Table 1
The above study experimentally derived the influence of the hydrophobic and hydrophilic surfaces in Cellulose I-β nanocrystals on the behavior of CNC suspensions based on Hansen Parameters and sedimentation tests using binary mixtures and 59 solvents. It can be understood that the presence of hydroxyl groups promotes the dispersion of nanocellulose in a polar media, when compared with the surface energies[26, 27, 28] with these facets it becomes apparent that the polar and hydrogen bonding Hansen Parameters also contribute to the surface energy of a crystal plane along with the dispersion components.
Thus, the absolute differences in Hansen Parameters of the solvent and nanocellulose reflect upon the absolute differences in the surface energies of the solvent and nanocellulose, which has been highlighted by the work of Bergin et al[29], where the Flory Huggins parameters have been related to the surface energies rather than the cohesive energy. This approach has experimentally verified by[30] through their studies on the stability of CNT dispersions and[31] for Nanocellulose.

$$\Delta H_{mix} = \frac{2\phi(\delta_{NC} - \delta_{Sol})^2}{r} \tag{20}$$

Thus, based on the thermodynamic understanding of Free energy of mixing the dispersion stability of Nanocellulose colloids can be predicted in a quantitative manner using the Hansen Parameters or Surface Energy. In this regard as discussed above equation 10 plays a pivotal role in the prediction of interaction between solvent and nanocellulose, a lower value of R describes better dispersibility. Different solvents and their binary mixtures can be studied using this method as discussed in the next section.
Based on the understanding of the applicability of the Hansen parameters, dispersion behavior

of Nanocellulose in common solvents such as Water, MeOH, EtOH, BuOH, DCM, Toluene, and Heptane can be observed in existing literature[32]. It is observed that the trends predicted using the Hansen Parameters is per the experimental data in most of the cases, deviations from the expected trends are observed for Water.
Such deviations can be explained in terms of surface functionalization of CNCs and CNFs during acid hydrolysis and TEMPO oxidation, leading to electrostatic stabilization[32, 33, 34].

1.2.2 Electrostatic stabilization

As discussed in the previous section how electrostatic stabilization often is the cause for the deviation from the predictions of the Hansen parameter model and play an important role in colloidal stability. In this section the role of electrostatic stabilization shall be explored through the measure of Zeta potential ζ and how various process parameters, pH, and salt concentrations affect the surface charge formation and thereby affecting the zeta potential and electrostatic stabilization. The general stability of colloidal systems is controlled by the interaction potential V between the particles and by the size of the energy barrier ΔV. Aggregation is inhibited for an extended period if the energy barrier significantly exceeds the thermal energy k_BT, where T is the absolute temperature and k_B is the Boltzmann constant. On the other hand, aggregation occurs if the energy barrier is lower than k_BT.[12]
The synthesis route of the nanocellulose greatly affects the Zeta potential. CNCs are obtained through acid hydrolysis of a cellulose source, the choice of acid for the hydrolysis process and time of hydrolysis is a determining factor in colloidal stability of CNCs. Sulphuric acid hydrolyzed CNCs have been reported to have higher absolute zeta potential than of Phosphoric acid followed by Hydrochloric acid. This phenomenon can be explained by the presence of more surface charge density due to the higher degree of esterification by sulphuric acid followed by phosphoric acid and the lowest degree for hydrochloric acid. These ester functional groups increase the surface charge density on the Nanocellulose in water and the colloidal particles undergo electrostatic stabilization. Other surface modifications such as substituting the hydroxyl groups by carboxymethyl groups have also been reported in the past. Depending upon the surface modification various values of Zeta potentials have been reported in the literature all of which converge towards stabilization of the CNC dispersion. However, on the other hand CNFs have been reported to have inferior stability in water and are prone to aggregation, this is because mechanical disintegration of the fibrils does not introduce any functional group that those already present thus the surface charge remains lower than that of the chemically modified ones. Pawcenis.et.al[35] studied 1 % w/v aqueous dispersions of HCl hydrolyzed CNFs at various hydrolysis times of 90,180 and 270 minutes. The colloidal stability in this study was studied through dynamic viscosities and then correlated with ζ values of these dispersions. After ultrasonication treatments there was 100-to-300-fold increase in viscosity,

which signifies an increase in nanocellulose agglomeration and shall be discussed at length in the later paragraphs in this section. The effect of pH on particle aggregation showed dispersions at neutral pH were more stable than the ones at acidic or alkaline conditions. The ζ values reported tome constant for acidic conditions irrespective of hydrolysis times and within the range of -4.3 mV to -4.7 mV. With a decrease in the concentration of H_3O^+, a max value of ζ is observed between the pH of 7 and 9, in this pH range however there was observed to be a drop in Zeta potential with increased hydrolysis times, which suggest increased aggregation for longer hydrolysis times. Park.et.al[36] reported longer stability of 1 month for TEMPO-oxidized Bacterial CNFs and a ζ values of 39.7,46.2 and 55.3 mV at pH values of 4,6 and 8. Similar results were reported by Qi et.al[37] for sulphuric acid hydrolyzed CNCs, with higher viscosities under acidic and alkaline conditions owing to the particle aggregation. All the values of ζ reported were negative because of the presence e of anionic sulfate ester groups, the zeta potential values varied from -45.1 mV to -17.5 mV in the pH range of 1 to 7, the protonation of the sulfate ester groups is responsible for the reduction in surface charge and thus drop in Zeta potential. In the alkaline pH range the values of ζ changes from -45.1 to -26.1 mV in the pH range of 7 to 13. The Na^+ ions shield the negatively charged species causing the electric double layer to shrink, this phenomenon is also known as counter ion condensation and shall be discussed in-depth later in this section. The influence of HCl in particle agglomeration was reported to be more than that of NaOH as the addition of NaOH disrupts the crystallinity and the loss of cellulose crystallinity results in less sensitivity to ions. The studies reviewed in this article observed increased stability in the addition of surfactants like CTAB, SDS, CMC, and PF-127[35].

Previous studies have been conducted on the effect of mechanical processing such as microfluidizing and ultrasonication by Andrade et.al [38]. This study shows interesting results for different processing parameters considered (shown in Table 3). Prior to microfludization the zeta potential was reported to be -28 mV, it should be noted that for stable colloidal dispersions an absolute ζ of 30 mV is required (Mirhosseni.et al), without any change in the chemical environment, in the aqueous environment of Bacterial CNFs tend to aggregate. The ζ was observed to decrease with the fiber length, thus the ζ decreased as the cellulose was subjected to increased microfludizatiuon and ultrasonication treatment times. These observations are also consistent with studies performed by Tonoli et al, on the CNFs from Eucalyptus kraft pulp, where the only milled CNFs were reported to have a ζ of -49.8 mV post sonication the Zeta potential changed to -19.1 mV. The similar relations between fiber length with ζ and colloidal stability are also reported by Tsalagkas et al, where for a BC suspension a value of -35.9 mV was reported prior ultrasonication, which changed to -21.8 mV after mechanical treatment. The study conducted by Andrade et.al however reported that the ζ changes closer to neutrality after consequent cycles of microfluidazation and ultrasonication. These trends can be explained by the generation of new surfaces that these mechanical treatments

create which lack charged surface groups, thus resulting in lower surface charge density, however further studies need to be carried out on understanding the exact reasoning for such trends. Another interesting correlation is the lowering of the Crystallinity Index upon ultra-sonic treatment, which can be explained using the hot-spot theory, where the cavitation phenomenon creates highly localized hotspots(formation, growth and collapse of microscopic vapor bubbles in a sequential manner), these hotspots in cold liquids drive high-energy reactions and interferes with the reorganization/recrystallization of Cellulose from a high-energy complex thus transforming crystalline zones into amorphous ones. The loss of crystalline phases also means the loss of the hydrophilic crystal facets as discussed in the previous section.

The effect of ionic strength was studied by Molnes.et.al[39] and showed as the ionic strength increased the dispersions gelation in the dispersions were initiated concluding particle agglomeration on increasing the ionic strength and reduction of zeta potential due to counterion condensation.[39, 16] The critical aggregation concentration decreased with increasing counterion valence. For the monovalent ions, the CACs followed the trend $Li^+ > Na^+ > K^+ > Cs^+$.[40]Thus its can be concluded that there exists a relation between the ionic size and zeta potential depression for the counter ion condensation phenomenon.

1.2.3 Phase Behaviour of Nanocellulose Colloidal Dispersion

Phase Behaviour of Nanocellulose Colloidal dispersions has been majorly studied through concentration-based transitions dependent upon the aspect ratio of the fibrils/rods[2, 41]. These transitions have been reported to be from a liquid state to a glassy and gel state with the characteristic G'>>G" and long chain relaxation time.

The caging or particle mobility constraint[42, 43, 44] imposed glassy state can be diluted back to the liquid state (reversed)[45, 46], along with the application of shear, changing the ionic strength or the temperature[42, 47]. Gels on the other hand are an attractive particle-particle interaction[42] volume arrested state with strong interparticle particle joints and bonds. The mechanism of such gel formation is the formation of fractal networks resulting from particle aggregation into percolated networks[42, 46]. Previous studies have reported the existence of a third state called attractive glass with the presence of both attractive and repulsive interactions, where repulsive interactions dominate the attractive one.[42]

These states undergo aging, a thermodynamically driven relaxation or rearrangement of particles for the reduction of free energy, in gels the particle-particle interaction increases to aggregate which decreases the free energy, whereas in glasses the particles rearrange in certain conformations to reduce free energy.[48]

Looking through an electrokinetic perspective, at a low surface charge there is a lack of electrostatic stabilization resulting in an aggregation of particles, the formation of volume arrested state is

thus due to the dominant Van der Waal interaction over the electrostatic repulsion, resulting in a net interparticle attractive interaction. For particles with high surface charge density, the electrostatic repulsion that is induced is sufficient to prevent aggregation at dilute and semi dilute concentration regimes, when the solvent is evaporated the counter-ion concentration increases thereby increasing the ionic strength and reducing the interparticle repulsion and gel formation. Depending on the counter-ion concentration, if the electrostatic stabilization is not sufficiently suppressed, the effective volume fraction is decreased with the reduction of Debye length due to increasing ionic strength thereby the liquid-glass concentration threshold is increased. Thus, in an arrested state the particle immobilization results in the presence of only vibrational and rotational movements and since such restrictions are caused by the double-layer overlap, the threshold concentration is inversely proportional to the aspect ratio.

The increasing concentration of the CNF dispersions leads to the formation of the colloidal glass state owing to the increasing mobility constraints, such constraints as explained earlier are guided by the effective volume of the rod/fiber particles(anisotropic) which depends on the surface charge density, aspect ratio, and counter ion concentration. Dilution of this arrested state leads to the breaking down of the larger structural networks which causes the dynamic arrest that result in a dispersion of smaller aggregates which can be classified as colloidal glass. Factors such as aggregation and colloidal stability influences the threshold volume fraction of the volume arrested state for different particle types, however the underlying cause of the Volume Arrested State is not attributed to the reduced colloidal stability, it is the mobility constraints that lead to formation of such states. On diminishing the surface charge at the volume arrested state particle agglomeration occurs leading to the formation of a gel structure that is resistant to dilution owing to strong Van der Waals attractive interactions.

The mobility constraints imposed in the volume-arrested states have been quantitatively studied through the Crowding Factor, which co-relates to the number of rods/fibrils that occupy a spherical volume with a diameter equal to the length of the rod/fibril and is given by,

$$N_{3D} = \frac{2}{3}\phi a^2 \tag{21}$$

where ϕ is the volume fraction and a is the aspect ratio of the nanocellulose. Such geometric models have been developed to study the arrested states based on the number of rods/fibrils and the volume of the blob they occupy[49]. As there is a transition from dilute to the semi-dilute regime, the particle-particle interaction increases such the spherical volume is occupied by only one rod/fibril i.e., a Crowding factor of 1, at this juncture the concentration at which the total volume of the unperturbed polymer coils is the same as the volume of the solution and is known as the Overlap Concentration[41, 50]. The sphere formed by the rotational volume overlaps beyond this concentration and hence there is an occurrence of a volumetric overlap concentration such that

the rotation of the rods/fibrils in 3D is constrained however translation and rotation in parallel is still allowed hence the system of the network is liquid. Particle interaction probability and the mobility constraints are directly proportional to the increase in concentration and mark the semi-dilute regime. These constraints gradually increase with the increase in concentration which results in a Newtonian-Viscoelastic transition and increase in viscosity.

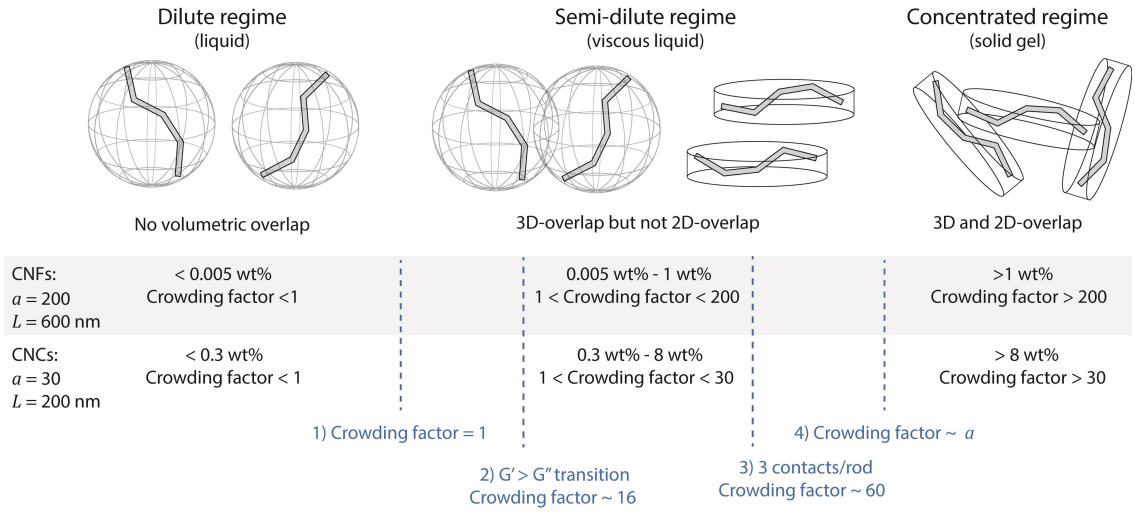

Figure 2: Concentration based transitions in nanocellulose colloidal dispersions , adapted from Benselfelt et.al [2]

From a solvent-nanocellulose interaction point of view, a theta solvent is a solvent where the fibrils/rods behave as ideal chains and is characterized by zero excluded volume at dilute concentrations with $\in_{cellulose-solvent} \gg \in_{cellulose-cellulose}$, $\in_{solvent-solvent}$ .From a thermodynamic understanding of the enthalpy of mixing for a theta solvent is zero and thus a solvent with Flory-Huggins Parameter $\chi \longrightarrow 0$, tends to behave as theta solvent. As discussed earlier, equation 9 and Equation 10 show that the solvent with Hansen Parameters equal to that of nanocellulose act as theta solvents. Scaling the behavior of 3D overlap concentrations for polymeric chains in theta solvent has been previously described to be $c^* \approx M^{-0.5}$, for good solvents $c^* \approx M^{-0.8}$ and $c^* \approx 1$ for bad solvents, where M is the molecular weight of the polymer chain. Thus, the selection of the solvent becomes of paramount importance in understanding of the imposed mobility constraints. Previous studies have reported four concertation-based phase transitions. A 3D overlap transitioning from dilute to semi-dilute regimes, a Newtonian to viscoelastic behavior transition in the semi the dilute regime, a transition beyond the rigidity threshold of 3 contact per rod/fibril and a Volume arrested state threshold due to 3D as well as 2D overlap, transitioning to a concentrated regime. As the aspect ratio of the CNFs increase the 3D overlap concentration decreases signifying a wider semi-dilute regime. An appropriate choice of solvent effects such transitioning point as discussed prior in this section. The aspect ratio is dependent on the source and processing of the nanocellulose,

Bacterial Cellulose has a high aspect ratio and nanocellulose derived from wood sources have a higher degree of modification resulting in low aspect ratio CNC and CNFs. Further shape factors and kinks in the fibrils play an important role in the formation of volume-arrested states, such that the crowding factor model shows a deviation from the experimental data by a factor of 1.5.[2]
The formation of the volume-arrested states does not completely restrict the fibril diffusion however the relaxation time for such movement/diffusion is long, overcoming the energy barrier of the network still results in a liquid phase, which is observed through the shear thinning behavior of nanocellulose dispersions. Under a shear strain, alignment of CNC/CNF fibrils occurs reducing the 3D mobility constraints allowing the flow of the dispersion[51]. Due to the maximization of the double-layer repulsion in the parallel conformation of the fibrils is energetically unfavorable, hence as the shearing stops the nanocellulose fibril/rod network due to rotatory diffusion and double layer repulsion returns to an orthogonal random or isotropic network[52]. The parallel configurations however remain stable in the case of nematic phases. The isotropic-nematic phase transition is associated with a tradeoff between the increase of translational entropy at the cost of rotational entropy, which is already restricted in isotropic orientation of higher volume fraction of nanocellulose, such configurational entropy tradeoff can be understood by the Onsager theory.[19]
Such conformational changes can be widely affected by the solvent, in the theta solvent, the radius of gyration scales differently than good and bad solvents. Additionally, in the case of charged particles, the size of the double layer and its effect needs to be considered and thus requires a modification of the Onsager theory[53, 54]. This order-disorder phase transition is dependent on the aspect ratio, taking into account the effective thickness due to the double-layer extension thus depending on the properties of the surface charge group properties and the electrolyte concentration.[55, 56]
The transition can be understood as the balance between the minimization of the excluded volume, the local osmotic pressure that guides the effective diameter of the rods/fibrils, thereby the effective volume occupied by the rods/fibrils and its counter-ion clouds i.e. the double layer overlap and relates to the total osmotic pressure when the excluded volume is considered. The local osmotic pressure owing to the excluded volume of polymeric chains is adversely affected by the choice of solvent. These transitions reduce the entropy of the system through a balance between the counter ion osmotic pressure and the translation freedom of the fibrils/rods. Such self-assembly is primarily driven by competing entropic and enthalpic interactions. The depletion interactions affect the local entropy that acts as a driving force towards such transitions.[57]
Rod-shaped nanoparticles and nanofibers at higher concentrations orient itself in parallel conformations for the minimization of the excluded volume of the isotropic/ random orientation, such phases are called nematic phases. The Isotropic phase is characterized with minimized overlap, maximized excluded volume, maximized ϕ_{eff} and is favorable at low-volume fractions, whereas the nematic phases are characterized by maximized overlap, minimized excluded volume, minimized ϕ_{eff} and

formation of nematic phases takes place at higher volume fraction.

The nematic transitions often start before the Volume-arrested state transition because of the effective diameter owing to the double layer repulsion. For low and moderately charged CNF like bacterial cellulose, the high aspect ratio and the kinks result in a low order of nematic phases before the VAS formation, this is a deviation from the ideal rod behavior. Such kinks have been attribute to the result of the mechanical treatment which defibrillation and not from the presence of amorphous regions in between regions of crystalline ones.[58, 59] Owing to the fact, CNFs are not straight rods like CNC or CNTs, they have kinks that make the possibility of cholesteric phases unlikely as the higher length scales of the fibril length cause a kinetic arrest and a direct transition to the volume arrested state from the dispersion with high relaxation time thus making the self-alignment into nematic phases difficult within a reasonable time frame. For theta solvents such transition to a kinetic arrest would happen at higher concentrations when compared to good and bad solvents, however in the past, there has been little to no study conducted on the phase behavior of nanocellulose using the thermodynamics of mixing and self-assembly through different solvent-nanocellulose interactions. Most studies have been limited to achieving stable CNF and CNC dispersions in various solvents.

For colloidal dispersions, a Flow Transition Index (FTI) shows the measure of the network behavior and its transition from Linear Viscoelastic regime to the state of flow, as the concentration increases beyond a threshold concentration, the FTI values close to 1 are associated with the embrittlement of the CNF dispersion[60] which is typical for nematic systems. The concentration beyond which the fraction of nematic domains is greater than the arrested fraction resulting in phase separation and weakening of the suspension network structure can be understood as the concentration beyond which the dispersion is no more stable. From earlier discussions in this section, it can be understood the effect of stability of the phase behavior of nanocellulose dispersions is not essentially a causative one but rather a limiting one, further controlling the solvent-cellulose interactions can improve the stability thereby the limiting factor.

Use of shear/ flow fields has been another approach that has been widely studied. Typically, the order-disorder of dispersions is studied through the order parameter, which is a quantification of the degree of ordered domains present. Hakansson et al[61] showed how to flow fields can achieve the alignment of CNF up to a maximum order parameter of 0.4 and in a separate study Mittal et al[62] reported a maximum order parameter of 0.5 with the use of flow fields. Torres-Rendon et al[63] achieved a maximum order parameter of 0.6 by wet stretching of wet spun CNF films. Extrusion followed by coagulation of CNF films also shows a similar order parameter of 0.6 as reported by Mohammadi et al[64]. As shown by Sehaqui et al [65], cold drawing of wet films can achieve the maximum order parameter of 0.7. Small brefingement regions under cross polarizers have been observed at concentrations as low as 0.5 wt% typically showing the formation of nematic domains[66], these however are locally aligned domains of fibrils and are not uniformly

spread. Concentration-based phase transition using flow fields of osmotic dehydration previously studied by Guccini et al[67]reported an initial concentration of 0.5 wt% carboxylated CNF dispersions with 0.6 mmolg^{-1} surface charge, the average aspect ratio of 125 being concentrated to 4.9 wt%, for concentrations above 1.7 wt % in the same study have been found out to increase the size of the nematic domains as they start coalescing. Small-angle X-ray scattering of such dispersions has shown in the past that a small fraction of the nematic domains are ordered, and the majority of such domains are isotropic. As the concentration increases the co-relation length of the polymer chain interactions arising from thermal energy decreases, thus resulting in the increasing relaxation time, and hence the fibrils become more closely packed. This phenomenon is like an isotropic shrinkage of a more generalized 3D network as there is a reduction of the fiber-fiber distance in the nematic domains, such conclusions can be drawn owing to the isotropic arrangement of the nematic domains. Depending upon the scaling of the characteristic size of the entangled region with the correlation length the presence of a fractal nature can be established, such power scaling is dependent upon whether the solvent is a theta solvent, good solvent, or bad solvent and hence whether the shrinkage/contraction as discussed above in the paragraph is affine or non-affine. The key element in the ordering and assembly of the nanofibers is the reduction of the network formation in the volume-arrested state such that the orientation of the CNF is facilitated while controlling its concentration. Such phenomenon can be attributed to the self-assembly kinetics and thermodynamic phenomenon between the fast diffusion-limited cluster aggregates and the slow reaction limited cluster aggregates[67] which is dependent on the trend the fractal dimension follows with the increase in concentration of nanocellulose. Formation of nematic ordered nanocellulose colloidal dispersions thus results from such trends that can be attributed to the Thermodynamic (solvent-cellulose interactions) and Electrokinetic interactions (kinetics of surface charge formation and counter ion concentration) which results in avoiding the restrictions imposed by the arrested state (longer relaxation times) and Hydrodynamic interactions (unidirectional flow fields) to orient the fibrils into nematic domains with higher order parameter.

1.3 Objectives and Thesis Overview

By investigating the complex interplay between the various intermolecular and surface forces governing CNF stability, aggregation, percolation, and assembly, this thesis aims to expand the systematic understanding of CNF colloidal prope ies to fulfill CNF's immense potential. A cross-disciplinary approach spanning polymer physics, colloid science, and rheology is undertaken to provide vital morphological, interactional, and flow characterizations.

The theoretical basis explores key factors like Van der Waal's forces ,entangled, networks, thermodynamic interactions, electrostatic repulsions, hydrodynamic regimes, and viscosity responses

to aid the future development of predictive models. Phase transformations in CNF dispersions are studied by tailoring variables like pH, ionic strength, and surface chemistry to reveal mechanisms for tuning stability. CNF-CNF and CNF-solvent interactions are probed by selectively varying solvent parameters and directly measuring viscosity signatures. Shear rheology thoroughly investigated to understand the concentration-dependent transitions spanning dilute suspensions to entangled networks to understand hierarchical assembly. Oscillatory experiments reveal relaxation phenomena, transient bonding, and dynamic moduli critical for structured material fabrication.

By holistically analyzing cellulose nanostructures across biosynthesis, nanoscale morphology, surface chemistry, colloidal interactions, rheological responses, and material microstructures, this thesis seeks to construct comprehensive roadmaps to guide CNF morphological control, optimized dispersion processing, and designed material fabrication to meet diverse application requirements in next-generation composites, biomedicine, and flexible electronics.

Objectives

The key objectives of this thesis comprise:

1. Characterizing the intermolecular forces like electrostatic and hydrodynamic interactions in CNF dispersions
2. Understanding the concentration-dependent phase behavior and transformations in CNF colloidal systems by selectively tailoring flow parameters.
3. Understanding the role of Thermodynamic interactions in Nanocellulose colloidal interactions and phase transitions through Rheology.

Thesis Overview

This thesis is structured across six chapters encompassing the theoretical background underpinning the prior research in this area, materials and methods, results, discussions, conclusions, and future work.

The introductory section establishes context and motivation regarding cellulose nanofiber colloidal behavior across thermodynamic, electrokinetic, and hydrodynamic interactions, colloidal phase transitions, and state-of-the-art standing. Pertinent dispersion behavior and material processing works spanning polymer physics and rheology are subsequently explicated as the theoretical basis along with characterization techniques.

Materials and experimental procedures entail CNF biosynthetic cultivation, fibrillation, purification, morphological analysis, and rheological investigations among others. Results reveal quantitative morphological attributes, surface chemistries, interaction mechanisms, and flow signatures

related to concentration transitions and network phenomena.

In-depth discussion contextualizes the fundamental insights regarding thermodynamic preferences, electrostatic stabilization, and hydrodynamic regimes in light of prevailing models, while conclusively synthesizing mechanisms and frameworks. Future work prospects highlight open challenges for simulation studies, complex interface constructions, and advanced manufacturing processes.

2 Materials and Methods

2.1 Materials

2.2 Experimental Methods

2.2.1 Growth of Bacterial Cellulose

Bacterial Cellulose was produced by inoculating blended commercially available kombucha starter scoby in 4 liters of freshly brewed tea media containing, 800 g of sugar (carbon source). After, inoculation, the broth was incubated at Room Temperature (25 °C) in a glass container under static conditions for 14 days. The container was covered with a muslin cloth to protect the growth of Bacterial Cellulose while maintaining airflow. The pellicle of cellulose formed at the air/liquid interface was harvested and purified under alkaline conditions by soaking the pellicle in 1 M NaOH for 24 hours, followed by immersing the pellicle in deionized water to remove the impurities till the pellicle turned white without blemishes and exhibited a neutral pH. The cleaned Bacterial Cellulose Pellicles were washed using hot water (90 - 100 °C) followed by crushing for 10 minutes using a Home Blender without adding any excess water. The blended suspension was moisture analyzed and diluted to a BC dispersion of 0.1 wt% using deionized water before blending further for 15 minutes. Part of the blended Bacterial Cellulose dispersion was then concentrated to 1 wt% using a dehydrator (32 C for 48 hours).

2.2.2 Preparation of Bacterial Cellulose Colloidal Dispersion

The 1 wt% dispersion was diluted to 0.031, 0.066, 0.125, 0.2 and 0.325 wt% by adding deionized water to characterize the Cellulose Nanofibers.

The 0.1 wt% dispersion was diluted to 0.075, 0.05, 0.03, 0.02,0.01, 0.0075, 0.005, 0.002 and 0.001 wt% dispersion by adding deionized water and IPA. Three sets of dispersion were prepared with interaction parameters 0.15 χ_w, 0.5 χ_w, and χ_w, where χ_w is the interaction parameter of water and cellulose. The dispersions were moisture analyzed to verify the final concentrations. All moisture analysis experiments were conducted in triplicates.
The Bacterial cellulose dispersions are referred to as CNF dispersions henceforth.

2.2.3 Preparation of Bacterial Cellulose Films

The Cellulose films were prepared by solvent-casting 0.1 wt CNF dispersion into molds. The solvent was removed by slow evaporation at 38°C in a dehydrator. Once the solvent was completely removed the films were taken out of the molds and hot pressed at 140°C at 5 kN for 15 minutes.

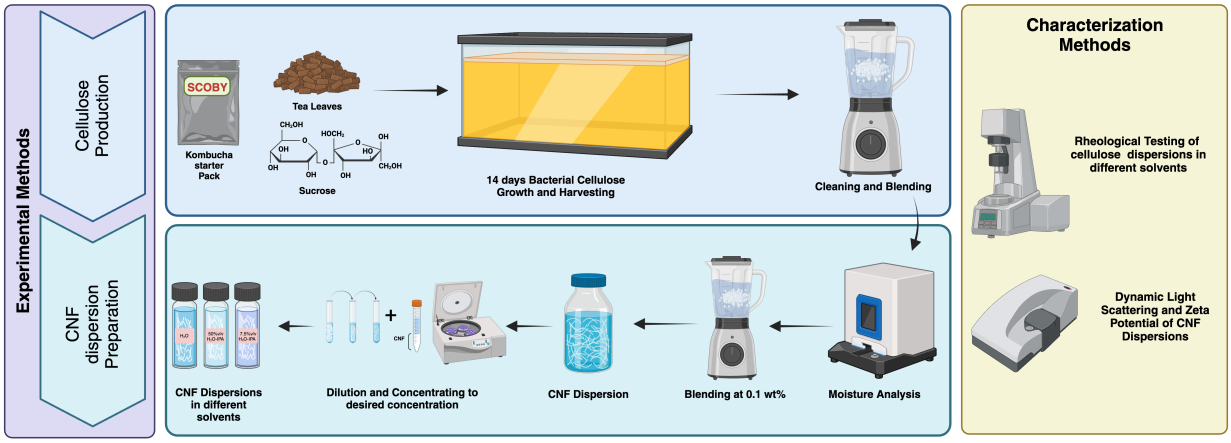

Figure 3: Schematic representation summarizing the key methodologies involved

2.3 Characterization Methods

2.3.1 Scanning Electron microscopy

50μL of 0.031 wt CNF dispersion was drop cast on a Silicon wafer using a pipette and dried under a vacuum desiccator. The SEM Image was captured using JEOL JSM-6010 Plus at the Material Science and Engineering Department, University of Washington. The Cellulose Nanofibers were imaged at a working distance of 11 mm, Energy intensity of 5kV, and spot size of 30.

2.3.2 Optical microscopy

The 0.031 wt CNF dispersion was dyed with Alcian Blue Dye and 100μL was cast on a glass slide, excess water was removed by gently placing a KimWipe at a corner and was then covered by a glass slide. The optical images were captured using a Motic B3 Series microscope under transmissive mode.

2.3.3 Surface Charge Density Measurements

The concentrations of the HCl, NaOH and NaCl are taken such that the ionic strength of the resulting solution always remains constant. 100g of 0.05 wt% BC dispersion in 0.2 mM HCl solution and 10 mM NaCl solution was titrated by 0.1 mM NaOH solution while simultaneously taking pH and conductivity measurements in triplicates.

2.3.4 Zeta Potential

The Zeta potential was measured by Dynamic Light Scattering using Malvern Zetasizer Nano ES at the Chemical Engineering Department, University of Washington. 0.005 wt% CNF dispersions

at pH ranging from 3 to 10 were prepared by adding 20 mM HCl and NaOH solutions, to keep the ionic activity constant 5 mM NaCl concentration was maintained for all the Zeta Potential Samples. The Zeta potential samples for CNF dispersions in different solvents were prepared in a similar method as mentioned above, however without the addition of any acid or base.

2.3.5 Rheological Methods

The 0.031 wt%,0.066 wt%, 0.125 wt%, 0.2 wt%, and 0.325 wt% CNF dispersions with water as the dispersant, were used for rheological characterization by Anton Paar MCR 301 Rheometer at the Chemical Engineering Department, University of Washington. A 25mm parallel plate Measuring System was used with a plate gap of 0.5 mm, a temperature for all experiments were carried out at a temperature of 25°C unless mentioned otherwise. The viscous response was measured under a Controlled Shear Rate, in the range of 0.01 s^{-1} to 100 s^{-1} with a measurement time of 15s and with measurement points varying linearly with the shear rate. Time-dependent viscous response against constant shear rate was measured at 0.01 s^{-1}, with an experimental time scale of 10 s, up to 300s, and with measurement points varying linearly with time. The hysteresis behavior of the CNF dispersions under simple shear was measured with a measurement time of 10s, with measurement points varying linearly with shear rate and in the shear range of 0.01 s^{-1} to 1 s^{-1}.The viscous response was measured in 3 intervals as the shear rate was ramped from 0.01 s^{-1} to 1 s^{-1}, then from 1 s^{-1} to 0.01 $s^{-1}$and again from 0.01 s^{-1} to 1 s^{-1}. For identifying the linear viscoelastic regime, an amplitude sweep from 0.5 % to 100% at a frequency of 1 Hz was run with a measurement time of 25 s and with measurement points varying with a slope of 7 pts/decade. Finally, the Frequency sweep was run at an amplitude of 5% from an angular frequency of 0.05 rad/s to 500 rad/s, with no time setting for measurement time and with measurement points varying with a slope of 5 pts/decade.
0.1, 0.075, 0.05, 0.03, 0.02,0.01, 0.0075, 0.005, 0.002, and 0.001 wt% CNF dispersions with water, 50 water-IPA, and 7.5 water-IPA were used for studying the effect of thermodynamic interactions, using the same Rheometer mentioned above but with Double Gap Measuring System. All the experiments were carried out at 25°C. The Frequency sweep was run at an amplitude of 1% from an angular frequency of 0.05 rad/s to 100 rad/s and the viscous response was measured under a Controlled Shear Rate, in the range of 10 s^{-1} to 1000 s^{-1} with a measurement time of 60s to 5s varying in logarithmic manner.

3 Characterization of Cellulose Nanofibers

3.1 Results and Discussion

In Figure 4, defibrillated CNFs can be observed in the SEM image, comparing the SEM image to the optical image, a hierarchical assembly of CNF fibers can be observed. From the SEM image, intuitively it can be understood that the diameter of the fibers is in the nanometer length scales, the CNFs is also observed to have kinks and bends and are highly entangled, which is characteristic of CNFs.

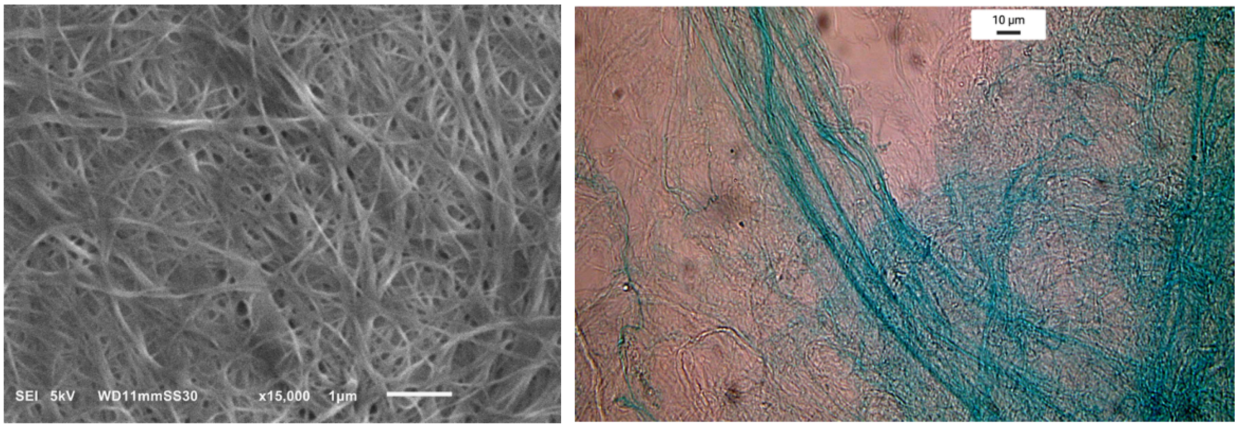

Figure 4: SEM Image of CNF dispersion (left), Optical Microscopic Image of CNF Dispersion (right)

3.1.1 Zeta Potential and Surface Charge Measurements

The Zeta Potential(Figure 5c) of CNF dispersions sheds light on the electrokinetic behavior of these nanofibrils in aqueous environments. The Zeta potential of CNF dispersions at pH 7 was measured to be -14.91 $\pm$ 0.55 mV, indicating the formation of negative surface charges in water. The value of Zeta Potential is also consistent with prior results for unmodified CNFs where the surface hydroxyl functional groups contribute to the zeta potential[68]. As the pH becomes acidic the absolute zeta potential reduces and under highly acidic conditions (pH of 3.5) a zeta potential of -4.07 $\pm$ 0.21 mV is observed, such suppression can be attributed to the protonation of surface charges by the H^+ ions. As the pH becomes basic, the absolute Zeta Potential value increases. At a pH of 9, a Zeta Potential value of -16.9 $\pm$ 1.6 mV is observed. Upon further pH increase to 10, the absolute zeta potential decreases to -11.18 $\pm$ 0.81 mV. This behavior is consistent with the prior works on the electrokinetic behavior of CNFs and can be explained by Manning's counter ion condensation (See section 1.1.3). As the counter ion concentration increases due to an increase in Na^+ ion concentration on the addition of NaOH, beyond a concentration there is a suppression in the Zeta Potential. The Zeta potential values signify that the colloidal particles are not stable

(generally stable dispersions are considered to have an absolute Zeta potential value $>$ 30 mV). This lack of electrostatic stabilization is due to the absence of functional groups that can dissociate into surface charges.

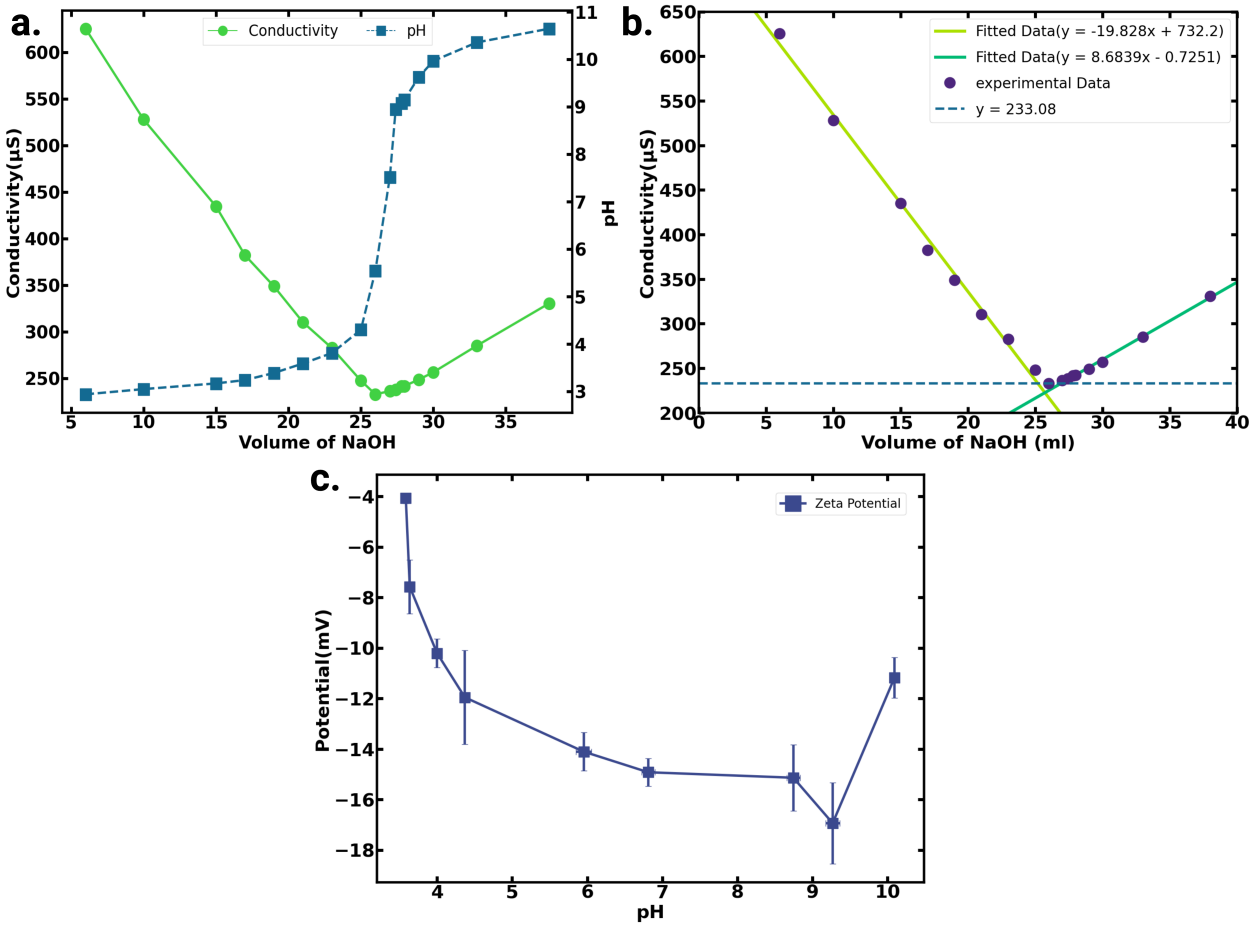

Figure 5: Conductometric Titration for the Surface charge Density Determination (a,b),Zeta Potential Variation with pH (c)

The surface charge density estimation further supports the Zeta Potential measurements. Figure 5a shows the constant conductivity region on adding NaOH solution before the conductivity increased again. This volume of NaOH was obtained to be 1.407 ml, by calculating the point of intersection of the lines relating to the decrease and increase of conductivity. This volume corresponds to 0.00028 mmole NaOH that neutralizes the developed surface charges in 100 g of 0.05 wt% CNF dispersion. Each mole of NaOH contributes as an equivalent mole of elementary charge e towards surface charge neutralization of the CNFs. Thus, the CNF in this study was measured to have a surface charge density of 5.63 mmol e Kg^{-1} or 0.00563 mmol e g^{-1}. Such low surface charge densities are consistent with existing literature where CNFs from HCl hydrolyzed Bacterial

Cellulose (no surface functionalization) was reported to have surface charge densities of the same order of magnitude[69]. Thus it can be understood that the low surface charge density results in low electrostatic potential thus, CNFs from Bacterial Cellulose, without any further surface modification have minimal electrokinetic contribution and are thus prone to aggregation or formation of agglomerates.

3.1.2 Rheology

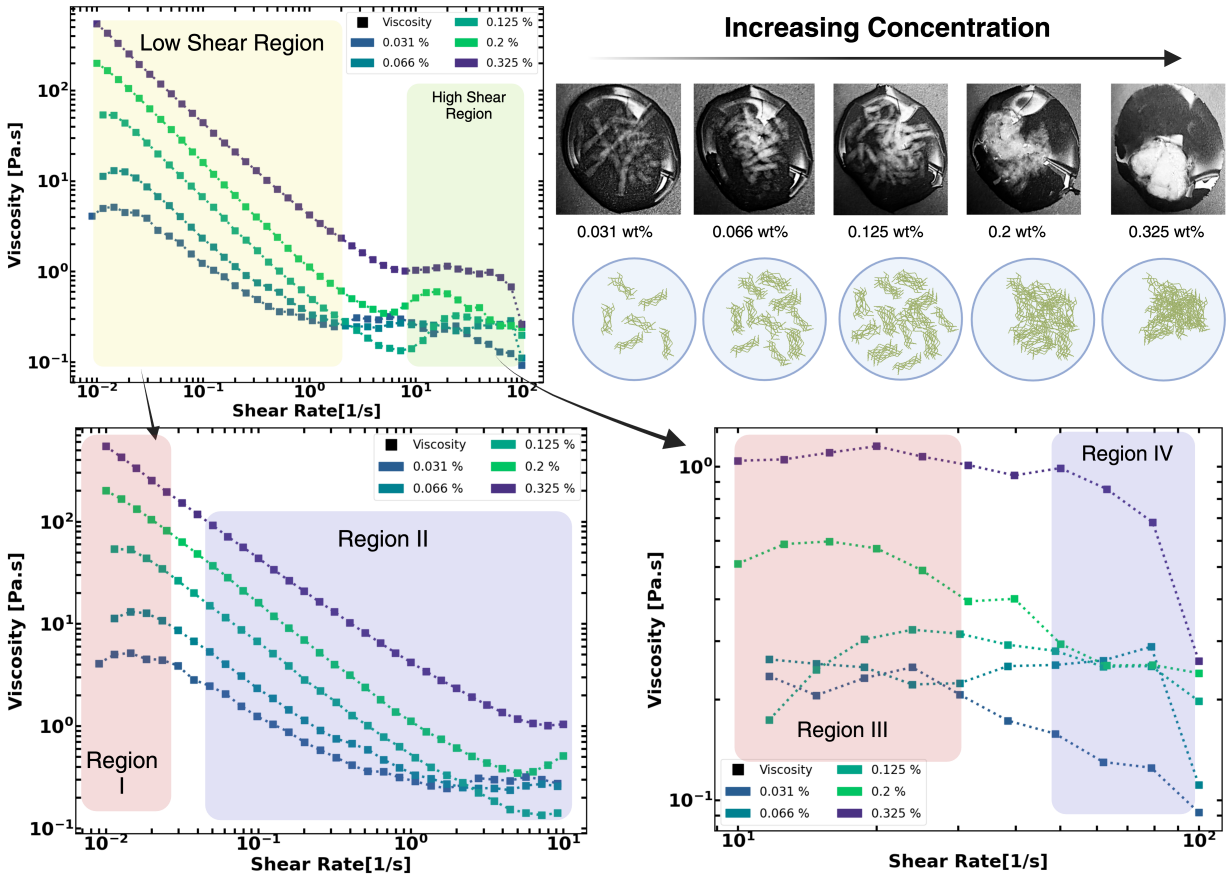

Figure 6: Viscous Response of CNF Dispersions, Viscosity vs Shear Rate Full Range (top left), Viscosity vs Shear Rate in Low Shear Regime(bottom left), Viscosity vs Shear Rate in High Shear Regime(bottom right), Optical Images of CNF agglomerates/hydroclustes after application of High Shear (top right)

The Viscous response of CNF dispersions typically shows four shear rate-based transitions which is consistent for CNFs as previously reported[70]. Firstly, a low shear rate Newtonian Plateau where the shear rate is much smaller for the fibers to overcome the entanglement as a strain is induced on the fiber. Beyond a certain critical threshold shear rate, the fibers start aligning in the shear direction, this is marked by a shear-thinning region. Once the fibrils are aligned in the

Conc (wt%)	$\eta_\circ$ (Pa.s)	η_{inf} (Pa.s)	λ (s)	n	R^2
0.031	5.12	0.244	25.31	-0.57	0.99
0.066	14.16	0.30	28.71	-0.77	0.99
0.125	72.08	0.35	55.66	-0.47	0.99
0.2	370.35	0.28	130.99	-0.23	1.0
0.325	2799.65	1.09	413.35	-0.13	0.99

Table 1: Carreau Fitting Parameters

shear direction a high-shear Newtonian Plateau is observed. This high-shear Newtonian plateau may be absent as seen in the cases of 0.031 wt%, 0.125 %, and 0.2 wt%, which is due to the occurrences of shear banding in the hydro clusters that are formed which lead to a slight increase in viscosity. A shear thinning behavior is observed again on further increasing the shear rate, where the hydro clusters align in the shear direction. As the concentration of the CNF is increased, the entanglements prevent the formation of a large number of hydro clusters. Rather, one large cluster is formed in those high-concentration cases, and that phase separates from the solvent at higher shear rates.

The viscous response of the dispersions has been modeled using the Carreau Model which provides an effective fitting for the viscosity as a function of the shear rate for polymer dispersions. The Carreau Model fitting is presented in Figure 7. The data is fitted from 0.01 s^{-1} to 1 s^{-1} to capture the first 3 regions accurately since the Carreau model does not take into account the formation of hydro clusters which is observed beyond the shear rate of 1 s^{-1}. Figure 7 depicts the Carreau model fitting and Table 1 summarizes the Fitting parameters. $\eta_\circ$ which is the zero shear viscosity was plotted against the volume fraction (right, Figure 5) and fitted in a power law equation, $\eta_\circ = a\phi^b$, where a is the constant coefficient and b is the scaling exponent and demarcates the concentration regimes in polymer physics. The $\eta_\circ$ first scaled $\approx \phi^{1.345}$ and then $\approx \phi^{4.134}$ both these scaling exponents are in agreement with the concentration-based semi-dilute and entangled regimes for athermal solutions/dispersions[71]. The semi-dilute and entangled regimes are demarcated by the entanglement volume fraction ϕ_e, beyond this increasing the volume fraction of the CNFs starts getting entangled with 3 contacts per fiber and represents the N_{3D}= 60. The onset of entanglement was calculated to be at a volume fraction of 7.034 $\times$ 10^{-4} which roughly corresponds to 0.11 wt % considering the density of cellulose to be 1.5 g/cm^3. Using Equation 21 (See 1.2.3) the aspect ratio was estimated to be 358. While this does not take into account the correction required for polydispersity, this method serves as a rough estimation for aspect ratio which otherwise is indeed difficult to estimate for longer CNFs like Bacterial Cellulose.

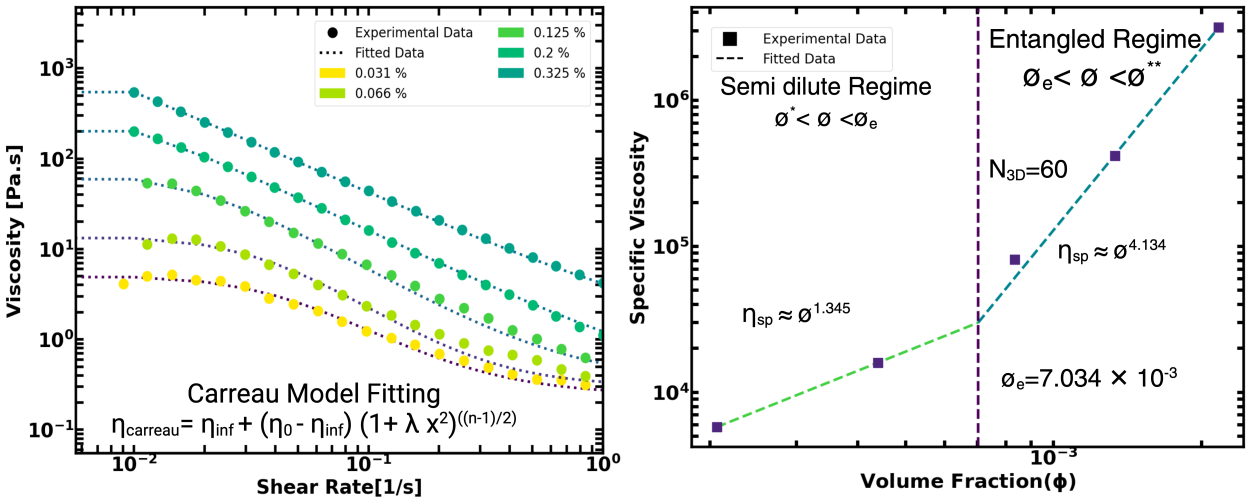

Figure 7: Carreau Model fitting (left), Zero Shear Viscosity Scaling with Volume Fraction (right)

The time-dependent structure properties(Figure 8) were characterized by applying a low constant step shear rate of 0.01 s^{-1} and instantaneous stress/viscosity response was observed over time. The total experimental timescale (t_{exp}) was 200 s with response to the constant load being observed every 10 s. Figure 5 depicts how the stress changes over time. For all the CNF dispersions, a linear increase in viscosity is observed followed by an overshoot in stress(viscosity), which gradually decreases till it reaches a steady state. In the context of time-dependent response, two-time constants play a vital role in the CNF behavior, the characteristic relaxation time(λ), which has been obtained by fitting viscosity against shear rate in the Carreau Model, as discussed above(Table 1), and the material structure time constant (t_{eq}), which depicts how fast the structure of a material change when a load is applied. The application of a low shear rate allowed studying the dispersions without instantaneous breaking of the structure, since for all concentrations at a shear rate of 0.01 s^{-1}, the viscosity is predominantly in the low shear Newtonian Regime (Region 1, see Figure 4). The stress overshoot is caused by a viscoelastic response of the CNF, upon reaching a critical strain, there occurs relaxation of the fibers resulting in stress decay. As the concentration increases, the overshoot becomes more pronounced due to increased entanglements and a stronger network structure.

Interestingly, new stress build-up is observed for 0.031 wt% and 0.066 wt% after the stress decay. This can be due to higher fiber mobility than the entangled dispersions which leads to the formation of the new structure in response to the applied load and thus stress build-up. Such fiber reorganization is not possible for the entangled regime and hence such behavior is not observed.

The Viscoelastic Properties of the CNF dispersions were studied using Oscillatory Rheology (Figure 9), and an amplitude sweep was performed to determine the limit of the Linear Viscoelastic

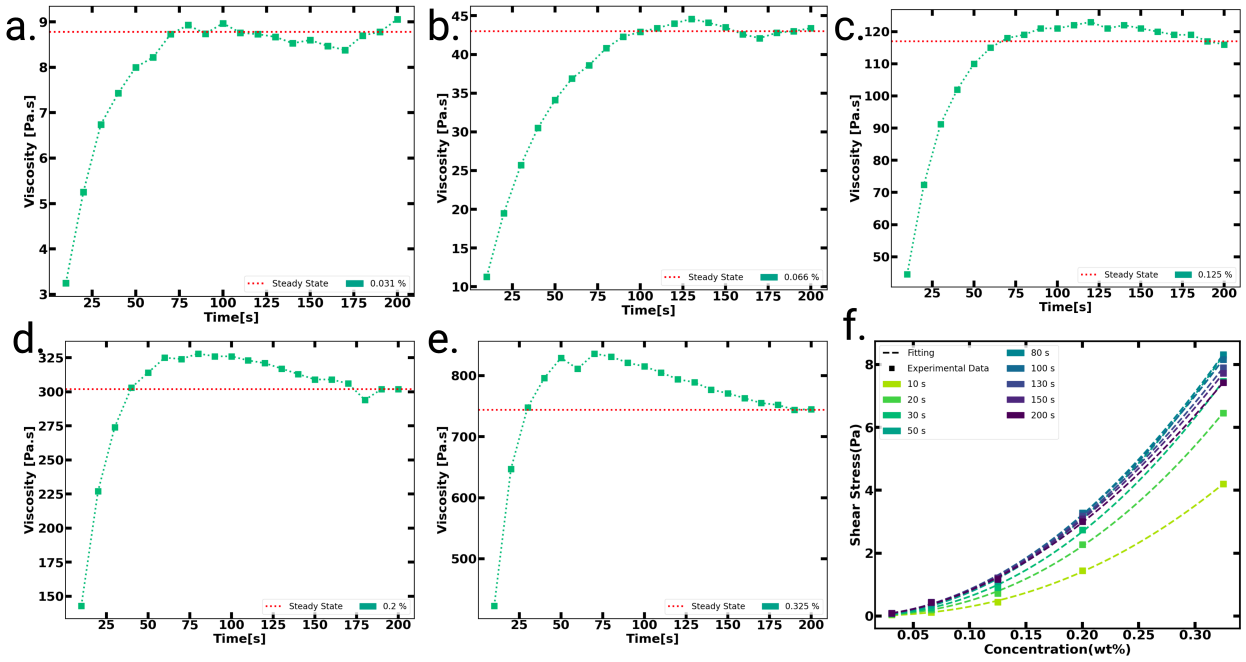

Figure 8: Time-dependent Viscosity response under Constant Shear(a -e), Power law fitting of Viscosity response against Concentration and Time (f)

Region ie a region where storage and loss moduli are independent of the strain amplitude. For the semi-dilute dispersions(0.031 wt% and 0.066 wt%) at low strain amplitudes, the loss modulus was near the limit of the instrument. Thus the non-linearity at the start is attributed to noise, which vanishes beyond 5% strain, and a linear loss moduli against strain is observed. All the dispersions exhibited a viscoelastic solid behavior owing to the gel network. Interestingly, the flow points, the critical strain at the material structure beaks down the viscous response dominates, varied inversely with concentration. This behavior can be attributed to the larger agglomerated structures/ formation of hydro clusters in the CNF network which is highly possible due to the lack of electrostatic stabilization(low surface charge density and low absolute zeta potential values) or non-uniform defibrillation due to mechanical blending. The Frequency sweep was performed at a strain amplitude that lie on the onset of non-linearity of the dynamic moduli. Frequency sweep at such large amplitudes sheds light on how the material structure breaks and thus the agglomerate structures. The $G' > G$" for all the dispersions and practically parallel to each other till a critical frequency threshold is reached and the network structure breaks down which is characterized by $G' < G$" and the CNFs flow with the viscous fluid-like behaviors while being entangled. The lack of a shoulder G' signifies an almost instantaneous breakdown of the network structure and brittle fracture of the CNF gels(observed in 0.066 wt% and 0.2 wt%), for 0.031 wt% and 0.125 wt% an increase in G' can be observed which corresponds to the formation of hydro clusters which justifies the sharp increase in complex viscosity at higher angular frequencies. In 0.325 wt% a shoulder can

be observed which signifies a gradual breakdown of the CNF network.

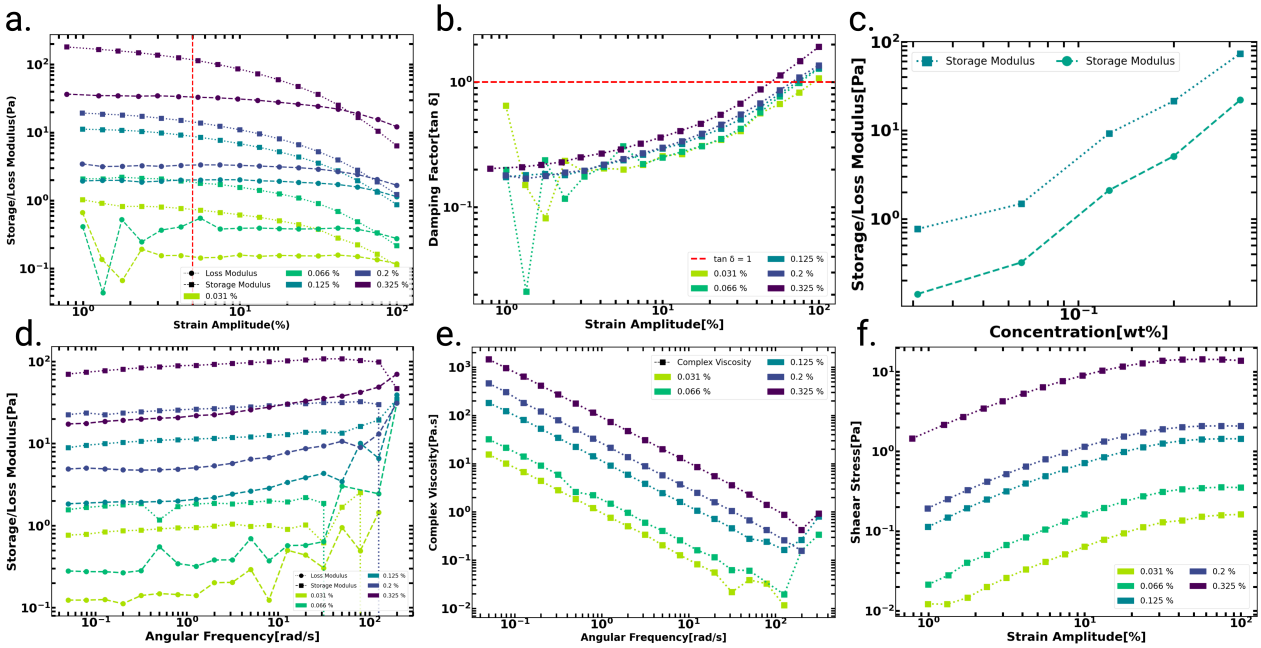

Figure 9: Loss and Storage Moduli over Strain Amplitude (a), Damping Factor(Tan δ) variation across Strain(b), Concentration Dependence of Loss and Storage Modulus at 1 % Amplitude and 1 rad/s Frequency(c), Frequency Sweep of Storage and Loss Modulus(d), Complex Viscosity against Frequency(e), Stress vs Strain(f)

3.2 Conclusion

This study elucidates the electrokinetic and rheological properties of cellulose nanofiber (CNF) dispersions in aqueous mediums. Zeta potential characterization demonstrates the effects of pH levels on CNF surface charge, revealing protonation and counterion condensation mechanisms. The low intrinsic surface charge density of unmodified CNFs, at 5.63 mmol e/Kg, suggests a tendency for aggregation without sufficient electrostatic stabilization. Concentration-dependent shear rate responses and hydrocluster formation are evidenced in rheology, with the Carreau model effectively capturing the viscous behavior and scaling of zero shear viscosity. The aspect ratio was determined to be around 358. The time-dependent properties showcase stress overshoots, relaxation behaviors, and viscoelastic effects such as linear regions and inconsistent flow points. The frequency responses further indicate network disintegration and agglomerate architectures mediated by concentration. By thoroughly investigating these fundamental electrokinetic and rheological characteristics of CNFs, this work provides critical frameworks and benchmarks to guide better control and tailored application of CNF dispersions across diverse industrial domains. The insights contributed lay the foundations for advanced material designs leveraging CNF colloidal interactions

and responses.

4 Cellulose Nanofiber Colloidal Properties

4.1 Results and Discussion

The three solvents used in this study are based on the Hansen Solubility Parameters, such that the interaction parameter χ can be minimized.

The χ parameter which is related to the Solubility parameters by equation 9 (see section 1.1.2), the Hansen Solubility Parameters of solvent were changed by adding IPA and Water to make 100%(solvent 1),7.5%(solvent 2), and 50%(solvent 3) water- IPA mixtures. The corresponding χ parameters were normalized by the interaction parameter of water and cellulose, thus resulting in cellulose-solvent interaction parameters being 1, 0.15,0.5 times that of the water-cellulose interaction parameter. This was done to get a semi-quantitative understanding of the thermodynamic interactions. On addition of IPA to water, the δ_h of the solvent was lowered thus ensuring that the hydrogen bonding solubility parameter of the solvent is close to that of Cellulose. The viscosity of IPA-Water mixtures was found from previous literature to be 2.6 mPa.s for solvent 3 and 2.15 mPa.s for solvent 2, similarly, the dielectric constant was found to be 20.95 for solvent 2 and 43.68 for solvent 3.[72]

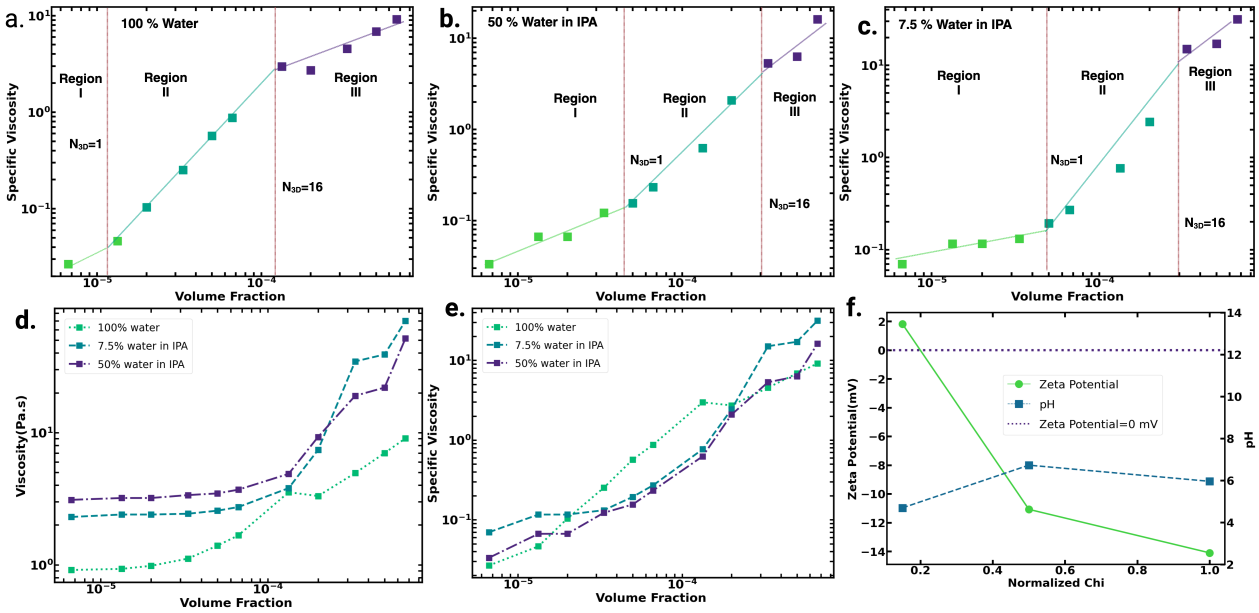

Figure 10: Specific Viscosity of CNF Dispersion showing Concentration based regimes at $316s^{-1}$ in 100% Water(a),50% Water in DI (b) and 7.5% Water in IPA(c), Viscosity in mPa.s against Concentration in the 3 solvents(d), Specific Viscosity against Concentration in the 3 solvents(e), Zeta Potential and pH of CNF dispersion in 3 solvents without addition of any acid/base(f)

Figures 10 a,b, and c show the Specific Viscosity scaling with Volume fraction of CNF in the different solvents, the specific viscosity variation with volume fractions graph has three distinct

regions based on slope changes on the log-log scale. The exact exponent of specific viscosity scaling with ϕ cannot be accurately fitted as done previously in Section 3.1.2. This is because in this case specific viscosity at 316 s^{-1} instead of zero shear viscosities that was used in Section 3.1.2 . At 316 s^{-1} considerable shear thinning occurs in volume fractions that lie in the semi-dilute regimes. Viscosity at 316 s^{-1} was used in this case as in the dilute and dilute-semi-dilute transitioning volume fractions, most rotational rheometers fail to accurately measure the viscosities at shear rates close to 0., However, the scaling exponent for Region I was close to 1 and between 1.3-2 for Region II for all the samples, which is consistent with previous literature[71, 50]. The slope changes even at such high shear rates however serve as a good indicator of the different concentration-based transitions, which have been used in the past to identify semi-dilute, entangled, and concentrated regimes. In such cases, most widely, shear rates of 100 s^{-1} have been used[50], in this study, we used a shear rate where viscosities of all three solvents can be measured, which was found to be 316 s^{-1}.

In solvent 1(100% water), Figure 10 a, the region I, corresponds to the dilute regime of polymer solutions and dispersions and is in good agreement with the aspect ratio characterized in Section 3.1.2. The predicted overlap concentration(c^*) ie the transition from dilute regime to semi-dilute regime occurs at N_{3D}=1, for an aspect ratio of 358, this corresponds to a volume fraction of 1.17 $\times 10^{-5}$ or 0.0017 wt% considering the density of cellulose to be 1.5 g/cm^3. At this concentration the total volume of the unperturbed polymer coils is the same as the volume of the solution, on further increase in the CNF volume fraction in region II, there is an increase in the mobility constraints and the dispersions transition into the region III, which marks the semi- dilute region where there is a Newtonian-Viscoelastic transition. This transition represents the 3D volumetric overlap, N_{3D}=16, and also corresponds well with the calculated aspect ratio in Section 3.1.2. and consequent Newtonian-Viscoelastic transition at a volume fraction of 1.17 $\times 10^{-4}$ or 0.0285 wt%. For Solvent 2 (7.5 % water in IPA) and Solvent 3 (50 % water in IPA), the slope changes show a dilute to semi-dilute, N_{3D}=1, transition at higher volume fractions than solvent 1. This is consistent with the Scaling behavior of 3D overlap concentrations for polymeric chains as discussed in Section 1.2.3. Cellulose-solvent pairs with a lower χ parameter will have higher overlap concentration. In Solvent 2 and solvent 3, the dilute to semi-dilute transition can be seen shifting from 0.0017 wt%(as is the case of Solvent 1) to concentrations between 0.0075 wt% and 0.01 wt%. The N_{3D}=16 transition also appears to shift from 0.0285 wt% to that of 0.05 wt%. Such shifts in concentration-based regime transitions are a clear indication of the effect of thermodynamic interaction parameters on the colloidal behavior of nanocellulose. It is also important to understand that equation 21, fails to predict the concentration-based transitions when the thermodynamic interaction parameter is changed. In the past, this relationship has been widely used for cellulose-water dispersions, how-

ever on changing the solvent (and thus the thermodynamic χ interaction parameter), transitions shift to higher volume fraction. One of the primary reasons for this would be that this relationship is more appropriate for stiff rods like structures like CNCs and not long semi-flexible CNF fibers, further, it doesn't take into account the interaction parameters which is instrumental in polymer physics on the scaling of overlap concentrations. Another interesting phenomenon to observe would be, at the N_{3D}=16 transition, the viscosity is rather constant even with the increase in CNF volume fraction before it increases again. This behavior can be attributed to the formation of hydroclusters with percolated networks, in a Newtonian-Viscoelastic transition there is a formation of the percolated network, at high shear rates the network breaks down and forms dense hydroclusters which can contribute substantially to the viscous response. Experimentally this transition of Newtonian to Viscoelastic regimes through oscillatory Rheological measurements is extremely difficult for CNF with such low charge density. The loss and storage modulus were inconsistent across the concentration for all the solvents, this is due to agglomeration and the presence of flocs that give rise to G' greater G" response even at lower CNF volume fractions.

The viscous response of CNF dispersions culminates from the balance of the intermolecular forces arising from polymer-solvent,solvent-solvent, and polymer-polymer interactions which has been discussed in depth in section 1.1, with the CNFs considered as randomly arranged coils. The Relative viscosities (figure 11) increase with the increase in thermodynamic interaction parameter(χ) of the 3 solvents used in the study at low CNF volume fractions, showing the following trend, $\eta_{solvent2} > \eta_{solvent3} > \eta_{solvent1}$ where, $\chi_{solvent2} > \chi_{solvent3} > \chi_{solvent1}$. In the Dilute regime, the CNFs are widely separated and have no hydrodynamic interaction, for a solvent with a lower χ parameter, the solvent molecules interact and penetrate the coils more increasing the excluded volume. and thus causing an increase in Relative Viscosity. On increasing the χ interaction parameter, the polymer-polymer interaction forces increase and cause a reduction in the excluded volume which is marked by a reduction in Relative Viscosity.
In the Semi-Dilute region, the volume fraction of the CNF coils increases and starts hydrodynamically interacting and competing for space with one another. In thermodynamically superior solvents the excluded volume reduces on increasing the volume fraction of CNF till an upper boundary reaches a minimum excluded volume, because of the greater volume of coil contraction available this semi-dilute window is wider than thermodynamically inferior solvents. Further, increase in the CNF volume fraction the fibers are crammed together and there is an overlap(See Section 1.2.3), this increases the intermolecular forces especially the polymer-polymer interaction forces thus for solvent 1 there is a rapid increase in the viscosity compared to solvent 2 and solvent 3. Such behavior conforms well to the established understanding of polymer rheology.[73]. Interestingly however, there is a deviation from the ideal trend of $\eta_{solvent1} > \eta_{solvent2} > \eta_{solvent3}$, based on the

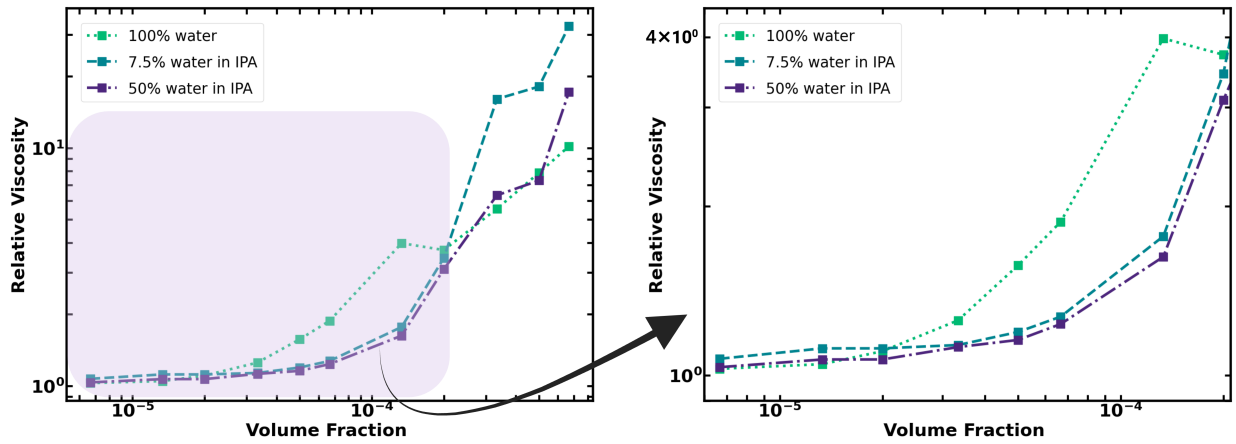

Figure 11: Relative of the different solvents across CNF volume fraction(left), highlight region of the graph on the right showing low volume fractions (left)

trend in interaction parameter($\chi_{solvent2} > \chi_{solvent3} > \chi_{solvent1}$), in the semi-dilute region and concentrated based on the above understanding. This deviation can be explained by the presence of lower electrokinetic stabilization in solvents 2 and solvent 3 than in solvent 1. Figure 8 f shows the Zeta potential of CNF in the 3 different solvents at their natural pH(without the addition of any acid or base), the solvent 2 has a Zeta Potential of 1.82 $\pm$ 0.85 mV,-11.1 $\pm$ 0.61 mV for solvent 3 and -14.1 $\pm$ 0.75 mV for solvent 1, this results in stronger Van Der Waals attraction in the hydroclusters formed at the high shear rates, the trend of zeta potential is similar to that of Relative Viscosities at 0.1 wt% for the 3 solvents. Figure 12, shows the solvent substracted full X-ray scattering pro-

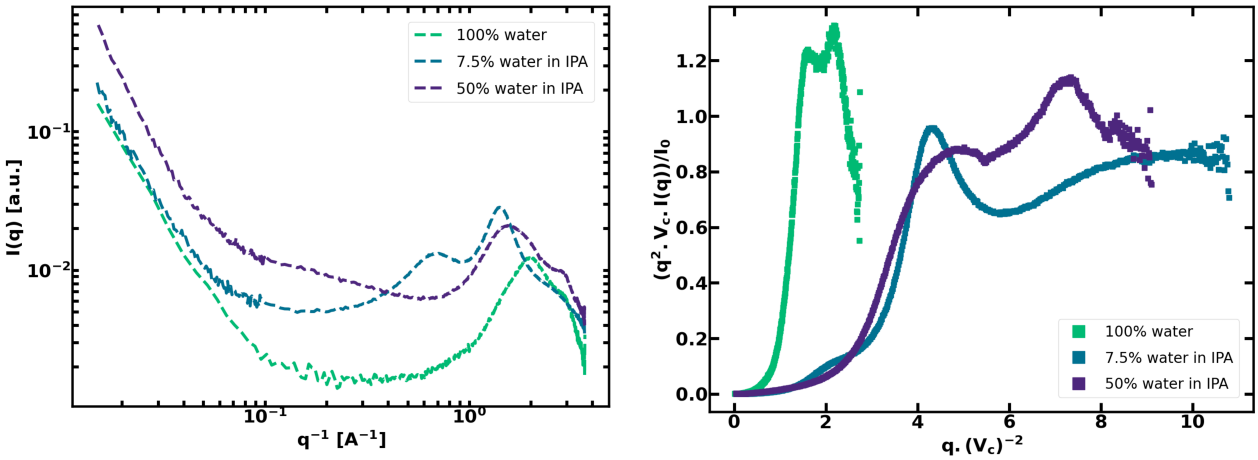

Figure 12: Solvent subtracted X-ray scattering profiles for 0.1 wt% CNF in the 3 different solvents. (right), Dimensionless(V_c) Kratky Plot (left)

file for 0.1 wt % CNF dispersion in the 3 different solvents and the Dimensionless Kratky Plot (Normalized to take into account the size effects). For solvent 1 (100 % Water) dispersions, the

Solvent	Normalized χ (χ/χ_w)	Zeta Potential(mV)
100 % water	1	-14.1 $\pm$ 0.75
7.5 % water in IPA	0.15	1.82 $\pm$ 0.85
50% water in IPA	0.5	-11.1 $\pm$ 0.61

Table 2: Table summarising the Zeta Potential for CNF dispersions in different solvents

Katky plot is typical for a much globular-like structure, which is due to the CNF fibers contacting and collapsing onto each other due to stronger CNF-CNF interaction than CNF-solvent interaction, which is characteristic of Thermodynamically inferior solvents. For solvent 2 (7.5 % DI in IPA) the Kratky plot is characteristic for multi-domain semi-flexible polymer chains, and for solvent 3(50 % DI in IPA) the Kratky plot is typical for a multidomain extended chain. This behavior of the CNF fibers in these two solvents can be attributed to the lack of electrokinetic stabilization in Solvent 2 dispersions which is almost close to 0 mV, on the other hand, solvent 3 has relatively low but some electrokinetic stabilization that prevents the chains from folding on to itself. Thus the Kratky plot helps us confirm that the thermodynamic interactions have a profound impact on the CNF chain conformation resulting in differing colloidal behaviour.

From the Rheological, Zeta Potential, and x-ray scattering measurements, it can be concluded that thermodynamic interactions play an important role in the colloidal behavior of CNFs, however, it is important to understand that the thermodynamic, electrokinetic, and hydrodynamic interactions act in tandem with one another towards nanocellulose colloidal behavior.

4.2 Conclusion

This study reveals valuable insights into cellulose nanofiber CNFs' dispersion behavior in solvents with varying thermodynamic interaction parameters. Specific viscosity measurements showcase concentration-based transitions from dilute to semi-dilute regimes for each solvent, with 3D volumetric overlap concentrations shifting to higher CNF volume fractions for solvents with lower interaction parameters. Relative viscosity increases correlate with higher interaction parameters in dilute concentrations, evidencing the role of excluded volume effects. As the normalized χ parameter decreases, the N_{3D}=1 transition shifts from 0.0017 wt% to concentrations between 0.0075 wt% and 0.01 wt%., while the N_{3D}=16 transition shifts from 0.0285 wt% to that of 0.05 wt%. Deviations in viscosity measurements occur in semi-dilute regimes, attributed to weaker electrostatic stabilization and stronger van der Waals attractions facilitating hydrocluster formation, as confirmed by zeta potential trends. Thus, while low thermodynamic interaction parameters favor coil expansion and viscosity rises initially, the decreased electrostatic repulsion enables dense hydrocluster networks to override expectations at higher concentrations. This comprehensive analysis reveals the delicate balance governing dispersion forces, with molecular interactions, electrokinetic

effects, and hydrodynamic properties intricately interplaying to dictate CNF responses. By elucidating concentration-dependent mechanisms, this work lays the groundwork for more controlled CNF dispersion preparation, predictive modeling, and tailored material fabrication across application domains.

5 Thesis conclusions

This comprehensive investigation substantially advances the fundamental understanding of cellulose nanofiber dispersions spanning growth to colloidal properties.
The complex interplay of thermodynamic, electrokinetic, and hydrodynamic forces governing CNF rheological responses provides a critical foundation for predicting colloidal behaviors. Concentration-based transitions in rheology and the delicate balance of thermodynamic interactions and electrostatic repulsions are revealed, enabled by tailored solvent parameter alterations.
Surface charge density quantification confirms the propensity of insufficiently stabilized CNFs for agglomeration while pH modulations highlight protonation and counterion condensation influences. Observed shear responses demonstrate the concentration mediation of transient networks and hydroclusters.

Effective modeling by the Carreau model helps relate the zero viscosity scaling to concentration-based regime transitions, revealing an aspect ratio of 358, fiber relaxation phenomena, flow points, and frequency behavior show how increasing the concentration results in network formation. This multi-faceted exploration of growth mechanisms, dispersion preparations, colloidal interactions, viscoelastic properties and film fabrication delivers benchmark characterizations and structure-processing-property connections.

The effect of thermodynamic interactions on the colloidal behavior of nanocellulose , to our knowledge, has been studied for the first time. Decreasing the normalized χ parameter results in the N_{3D}=1 shift from 0.0017 wt% to concentrations between 0.0075 wt% and 0.01 wt%., while a shift from 0.0285 wt% to that of 0.05 wt% for the N_{3D}=16 transition. Effectively, a reduction in the χ parameter results in the shift of the concentration-based regime transition, thus showing that controlling the thermodynamic parameters would lead to wider processing windows for nanocellulose colloids.
By comprehensively investigating cellulose nanofibers across the value chain from biosynthesis pathways to material fabrication, this thesis establishes the foundation of robust frameworks to guide morphology control, interaction tuning, and property enhancement for tailored applications across industrial domains from structural materials to flexible electronics.

6 Future Outlook

While this work significantly advances the fundamental understanding of cellulose nanofiber interactions, and concentration effects on the colloidal properties, it also opens avenues for future exploration to realize their immense potential.

In terms of fundamental research, further investigations can focus on corroborating the models and mechanisms proposed using advanced simulation studies and imaging techniques. Elucidating the kinetics and dynamics of aggregation, hydrocluster formation, and network disintegration can pave the way for more predictive frameworks. Further exploration into the Thermodynamic interaction parameter needs to be undertaken through studies on the changes in the enthalpy of mixing/dilution.

Additionally, research into novel surface functionalizations can build on the baseline surface charge density quantification provided here. Electrostatic and steric stabilization via tailored chemical modifications can promote dispersion stability while also modulating compatibility, reactivity and assembly behaviors.The processing-structure-property relationships needs to be established create to opportunities for designed material fabrication. Polymer blending, composites and nanocomposites with CNFs as functional reinforcements can produce smart multifunctional systems leveraging interfacial and percolation effects.Scalable manufacturing processes like extrusion, injection molding and additive manufacturing with CNF-based bio-inks can potentially be optimized using the rheological signatures identified. This can accelerate adoption in high-value arenas spanning multifunctional films, structural composites,flexible electronics, green packaging and biomedicine .

By delivering vital morphological, colloidal and rheological insights, this research lights the path ahead for advanced CNF investigations, interactive material constructions and scalable technology translation to meet sustainability challenges globally.

References

[1] A. Fiorati, A. Bellingeri, C. Punta, I. Corsi, and I. Venditti, "Silver nanoparticles for water pollution monitoring and treatments: Ecosafety challenge and cellulose-based hybrids solution," *Polymers*, vol. 12, no. 8, 2020.

[2] T. Benselfelt, N. Kummer, M. Nordenström, A. B. Fall, G. Nyström, and L. Wragberg, "The colloidal properties of nanocellulose," *ChemSusChem*, vol. n/a, no. n/a, p. e202201955, 2023.

[3] R. J. Moon, A. Martini, J. Nairn, J. Simonsen, and J. Youngblood, "Cellulose nanomaterials review: structure, properties and nanocomposites," *Chem. Soc. Rev.*, vol. 40, pp. 3941–3994, 2011.

[4] I. A. Sacui, R. C. Nieuwendaal, D. J. Burnett, S. J. Stranick, M. Jorfi, C. Weder, E. J. Foster, R. T. Olsson, and J. W. Gilman, "Comparison of the properties of cellulose nanocrystals and cellulose nanofibrils isolated from bacteria, tunicate, and wood processed using acid, enzymatic, mechanical, and oxidative methods," *ACS Applied Materials & Interfaces*, vol. 6, no. 9, pp. 6127–6138, 2014. PMID: 24746103.

[5] S. D. Bergin, Z. Sun, D. Rickard, P. V. Streich, J. P. Hamilton, and J. N. Coleman, "Multicomponent solubility parameters for single-walled carbon nanotubesolvent mixtures," *ACS Nano*, vol. 3, no. 8, p. 2340–2350, 2009.

[6] M. Kleman and O. D. Lavrentovich, *Soft matter physics an introduction*. Springer, 2003.

[7] A. D. McLachlan, "Effect of the medium on dispersion forces in liquids," *Discussions of the Faraday Society*, vol. 40, p. 239, 1965.

[8] J. H. Hildebrand, J. M. Prausnitz, and R. L. Scott, *Regular and related solutions: The solubility of gases, liquids, and solids*. Chapman & Hall, 1970.

[9] R. J. Hunter, *Introduction to modern Colloid Science*. Oxford University Press, 1993.

[10] M. Rubinstein and R. H. Colby, *Polymer physics*. Oxford University Press, 2008.

[11] C. M. Hansen, *Hansen solubility parameters a user's handbook*. CRC Press, Taylor & Francis Group, 2018.

[12] C. M. Hansen and K. Skaarup, "The three dimensional solubility parameter-key to paint component affinities: Iii; independent calculation of the parameter components," *J. Paint Technology*, vol. 39, p. 511–514, 1967.

[13] G. Cao, *Nanostructures & Nanomaterials: Synthesis, Properties & Applications*. Imperial College Press, 2008.

[14] R. J. Hunter, *Zeta potential in Colloid Science*. Academic Press, 1981.

[15] R. M. Brown, "The biosynthesis of cellulose," *Journal of Macromolecular Science, Part A*, vol. 33, no. 10, p. 1345–1373, 1996.

[16] G. S. Manning, "Limiting laws and counterion condensation in polyelectrolyte solutions i. colligative properties," *The Journal of Chemical Physics*, vol. 51, no. 3, p. 924–933, 1969.

[17] Q. Lei, K. Li, D. Bhattacharya, J. Xiao, S. Kole, Q. Zhang, J. Strzalka, J. Lawrence, R. Kumar, and C. G. Arges, "Counterion condensation or lack of solvation? understanding the activity of ions in thin film block copolymer electrolytes," *Journal of Materials Chemistry A*, vol. 8, no. 31, p. 15962–15975, 2020.

[18] L. M. Penafiel and T. A. Litovitz, "Counterion condensation and ionic conductivity," *The Journal of Chemical Physics*, vol. 96, no. 4, p. 3033–3038, 1992.

[19] L. Onsager, "The Effects of Shape on the Interaction of Colloidal Particles," *Annals of the New York Academy of Sciences*, vol. 51, pp. 627–659, May 1949.

[20] J. K. Dhont and W. Briels, "Viscoelasticity of suspensions of long, rigid rods," *Colloids and Surfaces A: Physicochemical and Engineering Aspects*, vol. 213, no. 2, pp. 131–156, 2003.

[21] S. Marceau, P. Dubois, R. Fulchiron, and P. Cassagnau, "Viscoelasticity of brownian carbon nanotubes in pdms semidilute regime," *Macromolecules*, vol. 42, no. 5, pp. 1433–1438, 2009.

[22] T. Sato and A. Teramoto, "Dynamics of stiff-chain polymers in isotropic solution: zero-shear viscosity of rodlike polymers," *Macromolecules*, vol. 24, no. 1, pp. 193–196, 1991.

[23] S.-Y. Ding and M. E. Himmel, "The maize primary cell wall microfibril: a new model derived from direct visualization," *Journal of Agricultural and Food Chemistry*, vol. 54, no. 3, p. 597–606, 2006.

[24] C. Yamane, T. Aoyagi, M. Ago, K. Sato, K. Okajima, and T. Takahashi, "Two different surface properties of regenerated cellulose due to structural anisotropy," *Polymer Journal*, vol. 38, no. 8, p. 819–826, 2006.

[25] J. Gu and Y.-L. Hsieh, "Surface and structure characteristics, self-assembling, and solvent compatibility of holocellulose nanofibrils," *ACS Applied Materials & Interfaces*, vol. 7, no. 7, p. 4192–4201, 2015.

[26] A. P. Heiner, L. Kuutti, and O. Teleman, "Comparison of the interface between water and four surfaces of native crystalline cellulose by molecular dynamics simulations," *Carbohydrate Research*, vol. 306, no. 1–2, p. 205–220, 1998.

[27] J. F. Matthews, C. E. Skopec, P. E. Mason, P. Zuccato, R. W. Torget, J. Sugiyama, M. E. Himmel, and J. W. Brady, "Computer simulation studies of microcrystalline cellulose β," *Carbohydrate Research*, vol. 341, no. 1, p. 138–152, 2006.

[28] D. F. Evans and H. Wennerström, *The colloidal domain: Where physics, Chemistry, Biology, and technology meet*. Wiley, 1999.

[29] T. Phan-Xuan, A. Thuresson, M. Skepö, A. Labrador, R. Bordes, and A. Matic, "Aggregation behavior of aqueous cellulose nanocrystals: The effect of inorganic salts," *Cellulose*, vol. 23, no. 6, p. 3653–3663, 2016.

[30] J. N. Coleman, "Liquid-phase exfoliation of nanotubes and graphene," *Advanced Functional Materials*, vol. 19, no. 23, p. 3680–3695, 2009.

[31] A. Ferguson, U. Khan, M. Walsh, K.-Y. Lee, A. Bismarck, M. S. P. Shaffer, J. N. Coleman, and S. D. Bergin, "Understanding the dispersion and assembly of bacterial cellulose in organic solvents," *Biomacromolecules*, vol. 17, no. 5, pp. 1845–1853, 2016. PMID: 27007744.

[32] M. S. Reid, M. Villalobos, and E. D. Cranston, "Cellulose nanocrystal interactions probed by thin film swelling to predict dispersibility," *Nanoscale*, vol. 8, no. 24, p. 12247–12257, 2016.

[33] C. Bruel, J. R. Tavares, P. J. Carreau, and M.-C. Heuzey, "The structural amphiphilicity of cellulose nanocrystals characterized from their cohesion parameters," *Carbohydrate Polymers*, vol. 205, p. 184–191, 2019.

[34] Y. Wang, Z. Yu, A. Dufresne, Z. Ye, N. Lin, and J. Zhou, "Quantitative analysis of compatibility and dispersibility in nanocellulose-reinforced composites: Hansen solubility and raman mapping," *ACS Nano*, vol. 15, no. 12, p. 20148–20163, 2021.

[35] S. N. Molnes, K. G. Paso, S. Strand, and K. Syverud, "The effects of ph, time and temperature on the stability and viscosity of cellulose nanocrystal (cnc) dispersions: Implications for use in enhanced oil recovery," *Cellulose*, vol. 24, no. 10, p. 4479–4491, 2017.

[36] D. Pawcenis, M. Leśniak, M. Szumera, M. Sitarz, and J. Profic-Paczkowska, "Effect of hydrolysis time, ph and surfactant type on stability of hydrochloric acid hydrolyzed nanocellulose," *International Journal of Biological Macromolecules*, vol. 222, p. 1996–2005, 2022.

[37] M. Park, D. Lee, S. Shin, and J. Hyun, "Effect of negatively charged cellulose nanofibers on the dispersion of hydroxyapatite nanoparticles for scaffolds in bone tissue engineering," *Colloids and Surfaces B: Biointerfaces*, vol. 130, p. 222–228, 2015.

[38] W. Qi, J. Yu, Z. Zhang, and H.-N. Xu, "Effect of ph on the aggregation behavior of cellulose nanocrystals in aqueous medium," *Materials Research Express*, vol. 6, no. 12, p. 125078, 2019.

[39] A. B. Fall, S. B. Lindström, O. Sundman, L. Ödberg, and L. Wragberg, "Colloidal stability of aqueous nanofibrillated cellulose dispersions," *Langmuir*, vol. 27, no. 18, p. 11332–11338, 2011.

[40] F. K. Andrade, J. P. Morais, C. R. Muniz, J. H. Nascimento, R. S. Vieira, F. M. Gama, and M. F. Rosa, "Stable microfluidized bacterial cellulose suspension," *Cellulose*, vol. 26, no. 10, p. 5851–5864, 2019.

[41] M. Nordenström, A. Fall, G. Nyström, and L. Wragberg, "Formation of colloidal nanocellulose glasses and gels," *Langmuir*, vol. 33, p. 9772–9780, Sep 2017.

[42] H. Tanaka, J. Meunier, and D. Bonn, "Nonergodic states of charged colloidal suspensions: Repulsive and attractive glasses and gels," *Phys. Rev. E*, vol. 69, p. 031404, Mar 2004.

[43] P. A. Buining, A. P. Philipse, and H. N. W. Lekkerkerker, "Phase behavior of aqueous dispersions of colloidal boehmite rods," *Langmuir*, vol. 10, no. 7, pp. 2106–2114, 1994.

[44] K. Kang and J. K. G. Dhont, "Structural arrest and texture dynamics in suspensions of charged colloidal rods," *Soft Matter*, vol. 9, pp. 4401–4411, 2013.

[45] B. Ruzicka, L. Zulian, E. Zaccarelli, R. Angelini, M. Sztucki, A. Moussa¨id, and G. Ruocco, "Competing interactions in arrested states of colloidal clays," *Phys. Rev. Lett.*, vol. 104, p. 085701, Feb 2010.

[46] E. Zaccarelli, "Colloidal gels: equilibrium and non-equilibrium routes," *Journal of Physics: Condensed Matter*, vol. 19, p. 323101, jul 2007.

[47] J. Appel, B. Fölker, and J. Sprakel, "Mechanics at the glass-to-gel transition of thermoresponsive microgel suspensions," *Soft Matter*, vol. 12, pp. 2515–2522, 2016.

[48] R. Zargar, B. Nienhuis, P. Schall, and D. Bonn, "Direct measurement of the free energy of aging hard sphere colloidal glasses," *Phys. Rev. Lett.*, vol. 110, p. 258301, Jun 2013.

[49] Y. Xu, A. Atrens, and J. R. Stokes, "A review of nanocrystalline cellulose suspensions: Rheology, liquid crystal ordering and colloidal phase behaviour," *Advances in Colloid and Interface Science*, vol. 275, p. 102076, 2020.

[50] L. Geng, N. Mittal, C. Zhan, F. Ansari, P. R. Sharma, X. Peng, B. S. Hsiao, and L. D. Söderberg, "Understanding the mechanistic behavior of highly charged cellulose nanofibers in aqueous systems," *Macromolecules*, vol. 51, no. 4, pp. 1498–1506, 2018.

[51] E. Lasseuguette, D. Roux, and Y. Nishiyama, "Rheological properties of microfibrillar suspension of tempo-oxidized pulp," *Cellulose*, vol. 15, pp. 425–433, 06 2008.

[52] T. Rosén, N. Mittal, S. V. Roth, P. Zhang, F. Lundell, and L. D. Söderberg, "Flow fields control nanostructural organization in semiflexible networks," *Soft Matter*, vol. 16, pp. 5439–5449, 2020.

[53] A. Stroobants, H. N. W. Lekkerkerker, and T. Odijk, "Effect of electrostatic interaction on the liquid crystal phase transition in solutions of rodlike polyelectrolytes," *Macromolecules*, vol. 19, no. 8, pp. 2232–2238, 1986.

[54] J.-M. Jung and R. Mezzenga, "Liquid crystalline phase behavior of protein fibers in water: Experiments versus theory," *Langmuir*, vol. 26, no. 1, pp. 504–514, 2010. PMID: 19736961.

[55] X. M. Dong and D. G. Gray, "Effect of counterions on ordered phase formation in suspensions of charged rodlike cellulose crystallites," *Langmuir*, vol. 13, no. 8, pp. 2404–2409, 1997.

[56] X. M. Dong, T. Kimura, A. Revol, and D. G. Gray, "Effects of ionic strength on the isotropicchiral nematic phase transition of suspensions of cellulose crystallites," *Langmuir*, vol. 12, pp. 2076–2082, 1996.

[57] B. C. Rocha, S. Paul, and H. Vashisth, "Role of entropy in colloidal self-assembly," *Entropy*, vol. 22, no. 8, 2020.

[58] I. Usov, G. Nyström, J. Adamcik, S. Handschin, C. Schütz, A. Fall, L. Bergström, and R. Mezzenga, "Understanding nanocellulose chirality and structure–properties relationship at the single fibril level," *Nature Communications*, vol. 6, p. 7564, Jun 2015.

[59] T. Saito, R. Kuramae, J. Wohlert, L. A. Berglund, and A. Isogai, "An ultrastrong nanofibrillar biomaterial: The strength of single cellulose nanofibrils revealed via sonication-induced fragmentation," *Biomacromolecules*, vol. 14, no. 1, pp. 248–253, 2013. PMID: 23215584.

[60] T. G. Mezger, *The Rheology Handbook: For users of rotational and oscillatory rheometers*. 2020.

[61] K. M. O. Hrakansson, A. B. Fall, F. Lundell, S. Yu, C. Krywka, S. V. Roth, G. Santoro, M. Kvick, L. Prahl Wittberg, L. Wragberg, and L. D. Söderberg, "Hydrodynamic alignment and assembly of nanofibrils resulting in strong cellulose filaments," *Nature communications*, vol. 5, p. 4018, June 2014.

[62] N. Mittal, F. Ansari, K. Gowda.V, C. Brouzet, P. Chen, P. T. Larsson, S. V. Roth, F. Lundell, L. Wragberg, N. A. Kotov, and L. D. Söderberg, "Multiscale control of nanocellulose assembly: Transferring remarkable nanoscale fibril mechanics to macroscale fibers," *ACS Nano*, vol. 12, no. 7, pp. 6378–6388, 2018. PMID: 29741364.

[63] J. G. Torres-Rendon, F. H. Schacher, S. Ifuku, and A. Walther, "Mechanical performance of macrofibers of cellulose and chitin nanofibrils aligned by wet-stretching: A critical comparison," *Biomacromolecules*, vol. 15, no. 7, pp. 2709–2717, 2014. PMID: 24947934.

[64] P. Mohammadi, M. S. Toivonen, O. Ikkala, W. Wagermaier, and M. B. Linder, "Aligning cellulose nanofibril dispersions for tougher fibers," *Scientific Reports*, vol. 7, no. 1, 2017.

[65] H. Sehaqui, N. Ezekiel Mushi, S. Morimune, M. Salajkova, T. Nishino, and L. A. Berglund, "Cellulose nanofiber orientation in nanopaper and nanocomposites by cold drawing," *ACS Applied Materials & Interfaces*, vol. 4, no. 2, pp. 1043–1049, 2012. PMID: 22257144.

[66] J. P. Lagerwall, C. Schütz, M. Salajkova, J. Noh, J. Hyun Park, G. Scalia, and L. Bergström, "Cellulose nanocrystal-based materials: From liquid crystal self-assembly and glass formation to multifunctional thin films," *NPG Asia Materials*, vol. 6, no. 1, 2014.

[67] V. Guccini, S. Yu, M. Agthe, K. Gordeyeva, Y. Trushkina, A. Fall, C. Schütz, and G. Salazar-Alvarez, "Inducing nematic ordering of cellulose nanofibers using osmotic dehydration," *Nanoscale*, vol. 10, p. 23157–23163, Dec 2018.

[68] N. E.-A. El-Naggar, A. B. A. Mohammed, and S. E. El-Malkey, "Bacterial nanocellulose production using cantaloupe juice, statistical optimization and characterization," vol. 13, p. 51, Jan. 2023.

[69] H. T. Winter, C. Cerclier, N. Delorme, H. Bizot, B. Quemener, and B. Cathala, "Improved colloidal stability of bacterial cellulose nanocrystal suspensions for the elaboration of spin-coated cellulose-based model surfaces," *Biomacromolecules*, vol. 11, no. 11, pp. 3144–3151, 2010. PMID: 20936805.

[70] E. J. Foster, R. J. Moon, U. P. Agarwal, M. J. Bortner, J. Bras, S. Camarero-Espinosa, K. J. Chan, M. J. D. Clift, E. D. Cranston, S. J. Eichhorn, D. M. Fox, W. Y. Hamad, L. Heux,

B. Jean, M. Korey, W. Nieh, K. J. Ong, M. S. Reid, S. Renneckar, R. Roberts, J. A. Shatkin, J. Simonsen, K. Stinson-Bagby, N. Wanasekara, and J. Youngblood, "Current characterization methods for cellulose nanomaterials," *Chem. Soc. Rev.*, vol. 47, pp. 2609–2679, 2018.

[71] J. Choi, K. S. Cho, and M. K. Kwon, "Self-similarity and power-law spectra of polymer melts and solutions," *Polymers*, vol. 14, no. 19, 2022.

[72] J.-G. Park, S.-H. Lee, J.-S. Ryu, Y.-K. Hong, T.-G. Kim, and A. A. Busnaina, "Interfacial and electrokinetic characterization of ipa solutions related to semiconductor wafer drying and cleaning," *Journal of The Electrochemical Society*, vol. 153, p. G811, jun 2006.

[73] T. Strivens, "14 - an introduction to rheology," in *Paint and Surface Coatings (Second Edition)* (R. Lambourne and T. Strivens, eds.), Woodhead Publishing Series in Metals and Surface Engineering, pp. 550–574, Woodhead Publishing, second edition ed., 1999.